PLANNAR MICROWAVE IMAGING SYSTEM

A THESIS IN ELECTRICAL ENGINEERING
Master of Science in Electrical Engineering

Presented to the faculty of the American University of Sharjah
College of Engineering
in partial fulfillment of
the requirements for the degree

MASTER OF SCIENCE

by
Mohammad Asefi
B.S. 2009

Sharjah, UAE
May 2011

PLANNAR MICROWAVE IMAGING SYSTEM

Mohammad Asefi, Candidate for the Master of Science Degree

American University of Sharjah, 2011

ABSTRACT

Microwave signals have shown a tremendous utility in a wide variety of applications. Due to their penetrative nature, one of the most exciting applications of all is utilization of microwave signals to see through dielectric structures. Among all, microwave non-destructive evaluation and inspection (NDE&I) of structures and materials is one of the most adopted techniques. Such techniques are primarily based on measuring coherent electric field distribution on the target being imaged.

In this thesis, the design, fabrication and measurement of a novel microwave imaging system, "a microwave camera", is presented. The design is based on a 10 GHz transmitter using a horn Antenna, an array of microstrip receiver antennas and a novel switching network. The received data is followed by a fast down converter to baseband and a custom-designed data acquisition system and GUI.

The system offers novelty in terms of operating frequencies, receiver antenna and accuracy of distinguishing between materials of various dielectric constants. The scanning and switching stage designed for this project is also new.

A prototype for the proposed system was also built and used to image objects of different materials and dielectric characteristics. Using the obtained results, the performance of the system was then analyzed.

CONTENTS

LIST OF ILLUSTRATIONS

LIST OF TABLES

ACKNOWLEDGEMENTS

The accomplishment of this thesis would not have been possible without the guidance and help of several individuals who in one way or another contributed and extended their valuable assistance.

I owe my most sincere gratitude to my advisors, Dr. Nasser Qaddoumi and Dr. Lutfi Albasha, for their support, encouragement, and immense knowledge. I would like to take this opportunity to thank Dr. Nasser Qaddoumi for all the support and knowledge he has given me throughout my study at this university.

Beside my advisors, I would like thank Dr. Yousef Al-Assaf, Dean of the Engineering College, for his support and motivation. I would also like to thank Dr. Mohamed El Tarhuni for his valuable help.

My thanks also go to Engineer I. Abuseif and Engineer W. El Tahir for their technical help and support and Engineer M. Narayanan for his help in PCB printing. Further thanks should also go to the manufacturing lab staffs for their help and efforts in fabricating some of the hardware.

During this work I have collaborated with my best friend, Engineer Soudeh Heydari Nasab, for whom I have great regard, and I wish to extend my warmest thanks to her for all her help and support.

On a special note, I would like to thank and extend my heartfelt gratitude to my parents for their unconditional love, endless support and encouragement. I am also thankful to my sister and brother for their encouragements.

To my parents, Asef Asefi and Tayebeh Zarei, whose advice and support has always lightened my life and paved my way to success.

CHAPTER 1

INTRODUCTION

The title of this thesis will be introduced briefly in this chapter. First a brief overview of microwave imaging will be presented. Later, the idea of how an active pseudo real time imaging system can be adopted in order to scan homogenous objects will be explained. At the end, the objectives of this thesis will be clarified and the general outline of the thesis will be provided.

1.1 Microwave Imaging

Looking around, it can be found that no matter where and in which field, there are applications that include microwave frequency signals, few examples of which are microwave ovens (as home appliances), cellular phones and satellites (as communication appliances) and etc. Among all, non-destructive and non-invasive imaging and testing methods exploiting microwave signals for the intention of material examination are quite well established and have been applied to different media [1],[2],[3],[4],[5],[6]. One of the main challenges of non-destructive methods is the increased use of composite materials for different applications in military, industrial, and medical fields. That is due to the non-homogeneous property of such materials [7]. However, such difficulties can be overcome by adopting multilayer imaging techniques with which different layers of a structure can be distinguished and imaged separately.

Basically, microwave imaging can be defined as scanning both an object and its internal structure by illuminating it with electromagnetic fields at microwave frequencies (300MHz – 300GHz) [8][9][10]. Generally, a microwave imaging system, also referred to as a microwave camera, includes a transmitter (typically an antenna) which is used to illuminate the structure under study with microwave signals. When these signals hit a structure, some of them will travel through with their phase and amplitude changed at the other side while some will reflect back with changes in their

magnitude and phase depending on the properties of the scanned layer of the structure. These altered signals can then be detected utilizing a sensor. The location of this sensor depends on the type of the imaging technique adopted (reflection or transmission through) [8], [11].

Furthermore, by changing the location of the structure under test (SUT) with respect to the illuminating source and the sensor, different layers of the structure can be scanned. This can also be achieved using an illuminating source at different frequencies. At the end, by processing the obtained data and using some reconstruction algorithms, different information about the complex dielectric permittivity and the shape of the scattering structure can be obtained. This thesis develops a system for such imaging scheme.

1.2 Motivation and Problem Statement

Seeing through non-conducting opaque materials and nondestructive evaluation (NDE) of structures are yet two of the most important achievements of the past few decades. Many techniques have been developed over years to provide new instruments that can reach such goals. Among the existing NDE techniques used in the past are use of eddy currents, ultrasound, and Radiography using X-ray or Gamma-ray. However, each of these techniques suffered from drawbacks. For instance, Eddy currents have limited applications since it can be used only in metallic structures while dielectric structures such as composite materials of plastics, ceramics, and carbon fibers replaced their metal counterparts in many applications. Furthermore, ultrasound's performance is highly degraded for inhomogeneous materials. Radiography using X-ray or Gamma radiation can effectively detect defects in the range of few micrometers; yet, it is costly, it has limited distance for ray penetration, and it has safety concerns.

Among all, most of the recent research is focused on use of microwave signals in such schemes. The capability of microwave signals to penetrate light opaque materials and sense distant or inaccessible objects with reasonable spatial resolution makes them attractive for different industrial, civil and medical applications. However, most of the techniques developed during the past years lack the capability of providing real time imaging as they use a single scanning probe. In this thesis, a

two dimensional microwave imaging system with which pseudo real time images of the internal layers of an opaque structure can be obtained is proposed and developed. This system is comprises of five main parts which are explained in detail in the following sections.

1.3 Methodology

In this thesis, a microwave imaging system comprising of an illumination unit, data gathering unit, down conversion unit, and a processing unit was proposed. Afterwards, each part of the system was designed, manufactured and tested separately. Results obtained from the tests are then be analyzed.

1.4 Thesis Outline

The chapters to follow are outlined as shown:

Chapter 2: This chapter provides the required background information on technical contents used in the later chapters. It also provides over view of techniques developed previously for microwave imaging.

Chapter 3: In this chapter an overview of the overall proposed system is presented. It also contains detailed description on selection, design and development of each part of the overall imaging system.

Chapter 4: Chapter four comprises two main parts; fabrication and system calibration, and testing. It starts by providing an overview on the adopted calibration method and it illustrates the obtained results. It also includes analysis on the obtained results from the tests. Moreover, this chapter provides an insight to the challenges faced during the manufacturing and calibration of each part.

Chapter 5: As the final chapter, it includes a summary of the final system design and the results obtained from system test. It also presents recommendations for future work.

CHAPTER 2

BACKGROUND AND LITERATURE REVIEW

In this chapter, a summary of the required literature review to understand the design of the proposed system is provided. Furthermore, this chapter includes brief description on some of the previously developed microwave imaging systems. The chapter starts by an introduction on nondestructive testing of dielectric materials. This section includes some of the previously developed methods for imaging an SUT via microwave signals. The chapter ends by briefly introducing some of the terms used throughout the presented work.

2.1 Non-destructive Testing (NDT)

One of the most active research areas of microwave imaging is nondestructive testing (NDT) measurements by which characterization of different materials (or structures) can be achieved. As the name suggests, using this method, one can get some information about an object, structure or even human body, without destroying it. These information can be about a material's characteristics (such as permittivity) or even about its internal layers (for instance, finding whether there is a defect in a material or not). Such information can be obtained by using nondestructive testing microwave imaging systems. Furthermore, the NDT can be utilized in the detection of defects in materials such as detection of cracks in concrete [8], [9]. The main principle behind these systems is that for a test structure (such as a concrete slab); a wave at a certain frequency, which is selected based on the skin depth of the material under inspection, will be transmitted through the object by a transmitting sensor, usually an antenna. In case a defect existed, the generated electric field will be disturbed at the location of the defect. This electric field distribution can be measured accurately by passing a short metal dipole through the field and recording the scattered wave by the dipole. However, this method has its own drawbacks some of which are critical tuning

adjustments, having a small scattered signal, and maintaining the stability of the dipole [9]. Later on, this method was improved by modulating the scattered field or in other words using modulated scattering technique (MST). This could be done by placing a nonlinear impedance at the center of a dipole and applying an audio voltage through slightly conducting threads which makes the relaxation of timing and stability requirements possible. Moreover, using this technique, the sensitivity of the measurements could be increased [10][12][13].

Breast tumor detection is one of the most active areas of research in which microwave cameras are being tried to work as tumor detection sensor. In these schemes, the presence of the tumor is to be found by analyzing the reflected signals from one's body. That is since the permittivity of the tumor and the rest of breast are different (Table 2.1) [21][22][23]. Figure 2.1 is a model of different layers and parts of the breast.

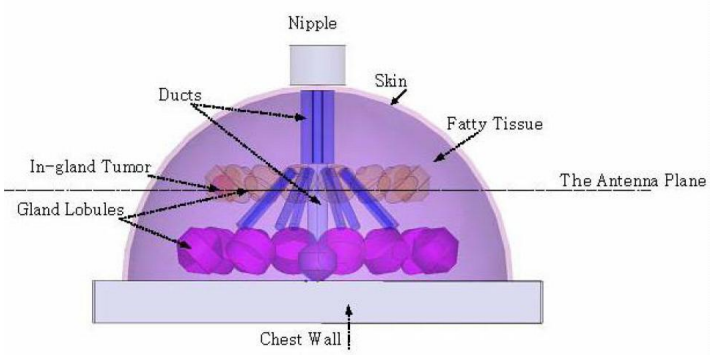

Figure 2.1 Different layers of breast [23]

Table 2.1 DIELECTRIC PARAMETERS OF BREAST TISSUES [21][22][23]

	ε_r	σ (s/m)
Skin	34.7	3.89
Fatty Tissue	9.8	0.4
Fibro-glandular Tissue	21.5	1.7
Ducts	37.96	4.5
Chest wall	55.56	6.5
Nipple	45	5
Tumor	50.7	4.8

In these schemes the main challenge is in the design of the sensor, frequency of operation-which cannot be higher than a certain amount due to skin depth of human

tissue- and the algorithm to be used to process the obtained data from reflected signals. Even though many good results have been achieved in this field, yet there are some concerns including limitations due to the fact that human body cannot be exposed to RF signals higher than a certain power (for more than a certain period of time) because of health issues.

2.1.1 Modulated scattering technique (MST)

Basically, the principle of MST is based on extraction of information from a reflected signal, which is caused by a scatterer placed at a point of interest, received by an antenna. The voltage obtained due to the presence of scatterer at a point will be proportional to square of the magnitude of the field at that point [12]. The signal coming from the scatterer (which is very small) can then be detected by a homodyne method. There are two basic schemes for measuring scattered fields, bistatic and monostatic (Figure 2.2).

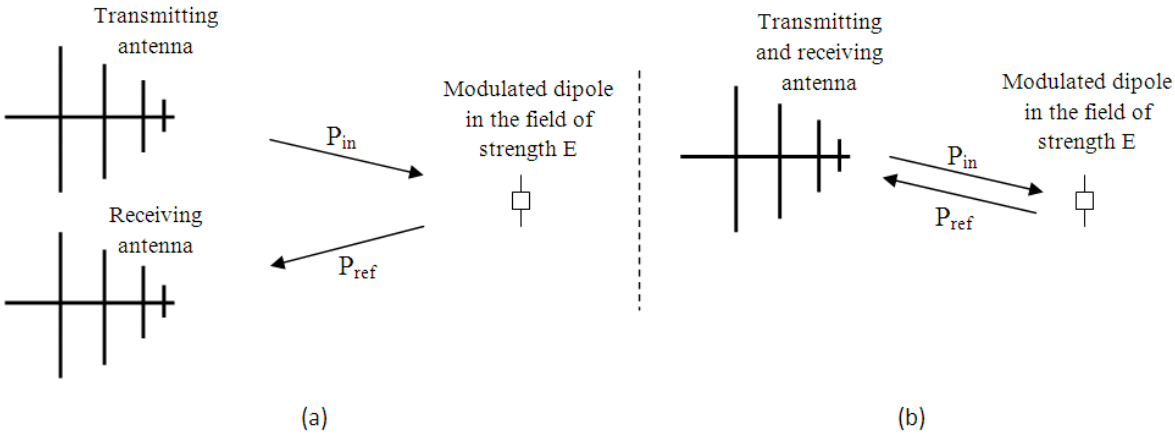

Figure 2.2 Scattered field measurement techniques (a) Bistatic (b) Monostatic

Typically, for the electric field detection a short (small) dipole is used, the modulation parameters of which usually consists in modulating its load. The load modulation thus causes modulation of the scattered fields [14], [15]. However, measuring the magnetic field can be done using a loop antenna.

In this technique, the scatterer can simply be modulated by switching its load between low impedance and high impedance. In MST, different types of switches can be used [12], the most popular of which are the diode (preferably Schottky) switches.

This system results in modulation of the signal with low frequency. Modulating the received signal at a low frequency has the advantage of decreasing the bulkiness of the system. Moreover, using this technique, the measured signal can be distinguished and spatially localized to the probe location by proper modulation and demodulation techniques[16]. Another advantage of MST is that, it requires only a single RF front-end and receiver, thus reducing the overall cost [17]. However, the small dipole used for this technique provides a very small modulation depth, which shows how much the modulated variable of the carrier signal varies around its unmodulated level. This limits the sensitivity and dynamic range of the overall system (which is typically between -40dBc to -70dBc) [16][18][19]. Furthermore, the signal transfer from the scatterer to the receiver is another issue with MST. That is, the overall system dynamic range is low since spatial collection schemes or passive combiners are lossy solutions [20]. Furthermore, the mutual coupling among the array elements (dipoles) can significantly limit system dynamic range. These problems become even more significant and challenging at higher frequencies such as those in the millimeter-wave region where there is a great need for rapid imaging systems at these frequencies.

2.1.2 Proposed system

Most of the previously developed microwave imaging systems mainly had a single standalone antenna as the transmitter and another as a receiver, while others used a transceiver where the transmitter and receiver use the same antennas and the reflection of microwave signals was analyzed to find the desired image. The design complexity and price of such schemes was high since they required very fast switching to avoid loss of information. However, such issues were overcome by latter designs where antennas were replaced by antenna arrays and in some designs the transmitter and receiver antenna arrays were placed next to each other (Figure 2.3) and reflected waves from the SUT was analyzed [24].

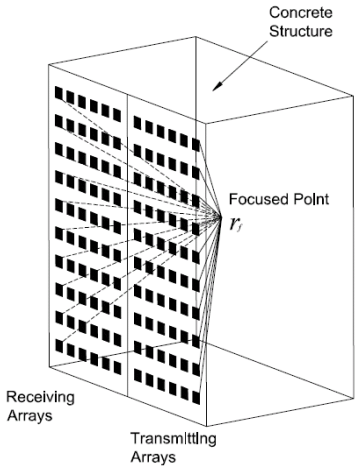

Figure 2.3 Transmitter and receiver antenna placed next to each other

Another example of systems using reflection method is arranging transmitting and receiving antenna elements in an interleaved manner as shown in Figure 2.4[16].

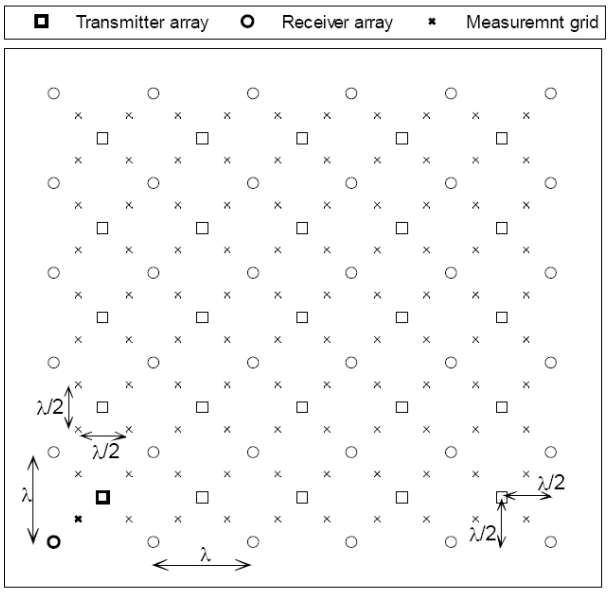

Figure 2.4 Transmitter receiver interleaved arrays

Although several imaging techniques have been developed, yet the system designs and imaging algorithms can be further improved and systems with different frequencies for other applications can be investigated. This thesis presents a 2d planner structure imaging system using microwave signals at 10 GHz. The aim of this work is to present a system that can scan a planner object and its internal structure and show a real time image of it. The main differences of this work from others are the frequency of operation, the antenna type and switching scheme, applications of use (imaging planner structures), and image processing and enhancement techniques. The

antenna array to be used as the receiver is going to have 64 elements, designed for operation at a frequency of 10 GHz, each being switched in a way that the image will be shown in real time with minimum delay. Moreover, the transmitter antenna will be an optimized standalone antenna placed at the other side of the structure to be imaged. For this purpose different antenna designs will be tested and analyzed to find the most efficient one.

2.2 Microwaves

Generally, alternating electromagnetic waves with frequencies varying between $300MHz$ and $300GHz$ with a wavelength of 1m and 1mm (with reference to the speed of light in free space $= 3 \times 10^8 m/s$) respectively, are referred to as microwaves[11] . The microwave spectrum is bounded by Radio frequency (RF) and Infrared (IR) frequency including ultra-high frequency (UHF), super high frequency (SHF), and extremely high frequency (EHF) signals (Figure 2.5).

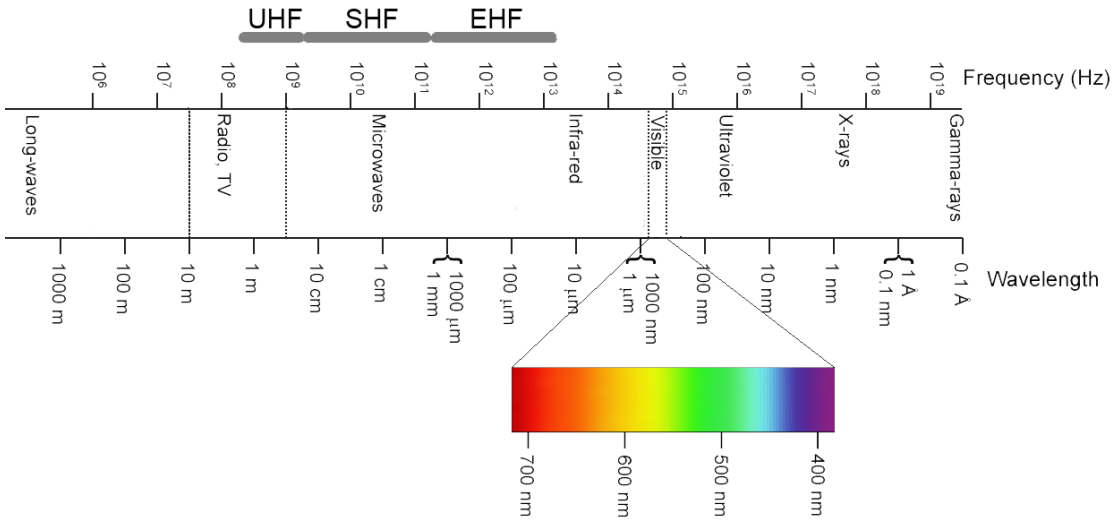

Figure 2.5 The electromagnetic spectrum showing the location of the microwave spectrum

Even though microwaves cover the frequency range starting from 300 MHz up to 300 GHz, yet most of the common applications are within the frequency range between 1 and 40 GHz which is classified as shown in Table 2.2:

Table 2.2 Microwaves Frequency bands.

Designation	Frequency range	Designation	Frequency range
L band	1.12 to 1.7 GHz	X band	8.2 to 12.4 GHz
R band	1.7 to 2.6 GHz	Ku band	12.4 to 18 GHz
S band	2.6 to 3.95 GHz	K band	18 to 26.5 GHz
H band	3.95 to 5.85 GHz	Ka band	26.5 to 40 GHz
W band	7.05 to 10 GHz		

2.3 Imaging Modes

Generally, imaging systems are classified into two main categories: near-field and far-field systems where near-field imaging requires the structure under inspection to be located close to the transmitter. On the other hand, in far-field imaging, the structure under study is required to be located far enough from the transmitter so that the waves propagated by the transmitter become planner waves.

These variations are due to the fact that antenna patterns vary in shape depending on the distance from the antenna and the angular direction. Depending on the relation of this distance with respect to the physical diameter of the antenna, two main regions are defined; near-field (Fresnel region) and far-field (Rayleigh region). The boundary between these regions can be determined by the Equation (2.1) [25].

$$R' = \frac{2D^2}{\lambda} \tag{2.1}$$

where,

R' is the distance determining the boundary between the far-field and near-field

D is the diameter of the smallest sphere that completely contains the antenna,

λ is the smallest wavelength of the transmitted signal.

2.3.1 Near-field imaging

To obtain substantially high resolution images, near-field techniques that operate less than 1 wavelength away from the image plane can be adopted. Generally, near-field region is referred to as the close-in region of an antenna where the angular field distribution is dependent upon the distance from the antenna [26]. Such techniques exploit the fact that the evanescent filed contains information beyond the

diffraction limit which can be used to construct very high resolution images. Evanescent field is referred to the near-field standing waves with an intensity that exhibits exponential decay with distance from the boundary at which the wave was formed [27]. However, since such techniques cannot image beyond 1 wavelength, their applicability is limited to imaging of objects thinner than one wavelength.

2.3.2 Far-field imaging

When imaging of structures larger than the illumination wavelength is of interest, Far-field imaging techniques are mostly desirable. This region is reached when the transmitter and the structure under test are located far enough from each other, where the shape of the radiation pattern over a sphere of constant radius becomes independent of R. This distance is known as the Rayleigh distance and it extends from the distance determined by the far-field condition of Equation (2.1) ($R \geq R'$). Thus, the target placed in this region is subject to plane waves. Mathematically, such region can only be reached at infinity which results in a finite wave front error in the far-field distance. In practice that is 1/16 of the smallest wavelength [28].

In this thesis, the focus will be to design a system that works in the far-field since it is to image structures larger than one wavelength of the transmitted signal. The system comprises of a waveguide (or horn antenna) as the illuminating source and an array of circular patch antennas as the receiving sensor with which a pseudo real time imaging system will be implemented and the structure under inspection will be monitored.

2.3.3 Types of Captured Images

In this design an open-ended waveguide is going to be used to radiate the required microwave signal toward the SUT. When a microwave signal hits the structure, depending on the dielectric characteristics of that structure, part of the wave will pass through and part of it will reflect back from the structure. The existence of this structure can affect both the magnitude and phase of the transmitted and reflected signals. The proposed system can measure both of these variations and generate three different types of images; magnitude, phase, and complex image.

Generally, magnitude images can be constructed from the intensity of the scattered signal, measured by the receiving antenna. However, phase images can be generated from the data obtained from measuring the phase variations in the scattered electric field due to existence of an object.

In order to obtain an enhanced image, both phase and magnitude images can be added together to form a complex image. Such image can have a higher contrast and provides a more visually desirable image of the structure under test.

CHAPTER 3

SYSTEM DESIGN AND CONSIDERATIONS

This chapter includes the proposed system and presents the theory and design behind each part of the proposed system. Generally, the system comprises of two main sections; hardware and software. The chapter begins by providing a brief description of the overall system. It continues with an explanation on the theory and the design of all hardware used for developing the system. This section contains description of the illuminating source, receiver sensor, switching scheme, and the down conversion and interfacing unit. This chapter will be finalized by explanation of the software and code developed for data analysis and image formation.

3.1 The imaging system hardware design

Imaging using microwave signals is based on the fact that electromagnetic waves experience different reflections when they penetrate different media. Monitoring the reflected signal (whether it is reflect through the object or reflected back from object) can provide information about the dielectric SUT. Different techniques can be adopted to detect and monitor this reflected signal. In this report, utilization of an imaging system with which the reflected through signal can be inspected is investigated.

This imaging system (Figure 3.1) consists of an oscillator, illuminator (transmitting antenna), receiver sensor (retina), switching unit, and a phase-magnitude separation and down conversion (demodulation) unit, and a processing unit.

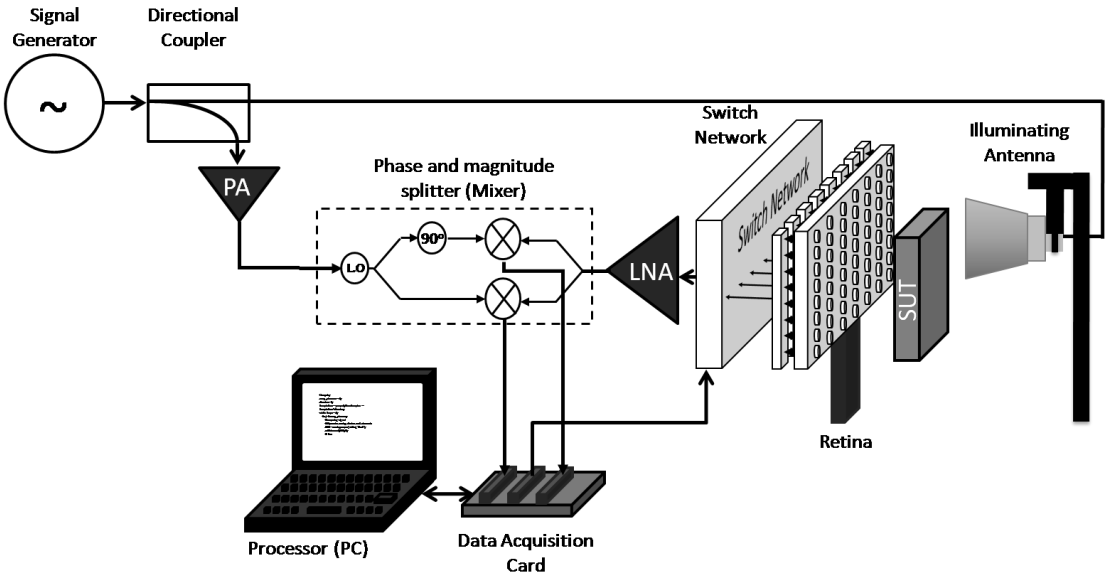

Figure 3.1 The proposed system diagram

In order to image a structure with this system, a high frequency wave, the frequency of which depends on the skin depth of that structure, is required to be transmitted through it. For the proposed two dimensional imaging system, a signal with a frequency of 10 GHz is to be used as the illumination signal and it is generated by a sweep oscillator. Later, this signal needs to be divided into two parts. This is done by a four port microwave component known as directional coupler (Figure 3.2) with a coupling factor of 0.1.

Figure 3.2 Directional Coupler

This means that 10% of the signal will pass through from port 1 to port 2. This signal is required as the reference for the down conversion unit to bring the received signal down to a DC level and make it ready for processing (i.e. it is to be used as the local oscillator signal of a mixer). The rest of this signal (which goes to port 3);

however, is to be used as the source of illumination and is fed to the transmitting antenna.

As for the antenna unit, two different transmitter and receiver antenna design and configurations are going to be studied. The first scenario is going to be adopting a single element transmitting antenna for which the transmitter can have any type as long as it satisfies the needs. While this technique is simple and easy to implement, there are certain drawbacks to it. On the other hand, there is a possibility of using a transmitter that comprises of array of antennas which is the same as that of the receiver. As the previous case, this system is also going to have some benefits and some drawbacks. The analysis of the performance of these two systems is going to further explored and the most beneficial type is going to be selected for the final system.

When this signal passes through a SUT, the reflected signal should be collected with a receiver sensor which is an array of antennas. That is since a two dimensional image requires information about the spatial coordinates of the data obtained from the scattered signal. By using an array of antennas, each element on the array can preserve the location of the signal it receives. Moreover, this type of receiver can provide a fast scan of different sections of the SUT. That is while a single element receiver antenna cannot provide a two dimensional real time image since it has to scan the whole structure which takes long time.

Basically, an image can be represented by a matrix that contains information of each pixel of the image, including the light intensity pixel, the color of the pixel and its location in the image. The values contained by each element of the matrix represent the images intensity and coloring information. That is while the location of each pixel is represented by the location of the matrix elements. This means that an image with higher quality (i.e. higher resolution image) will have a bigger representative matrix. Moreover, when an image of certain physical size has different resolutions (for instance an image with different compressions), its visual quality is going to drop as the resolution decreases (Figure 3.3). This means that if a certain visual quality is required, for different image resolutions the physical size of the image needs to change (i.e. as the resolution decreases, the physical size of the image should decrease to obtain the same visual quality as shown in Figure 3.4).

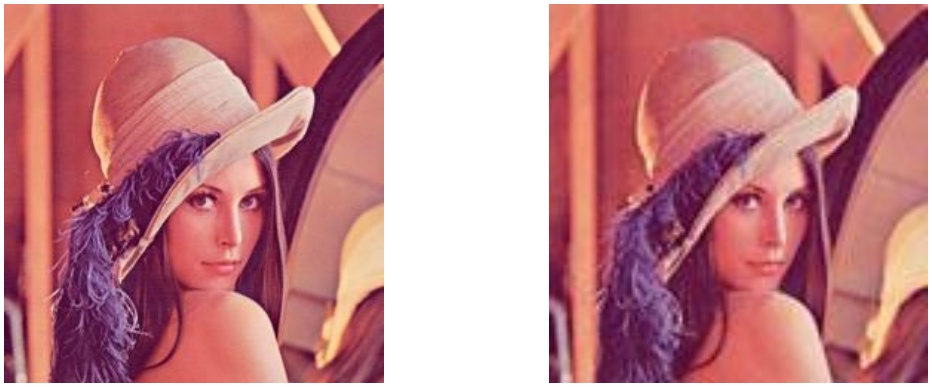

a)Original image (pixels: 256×256) b)Edited image (pixels: 128×128)

Figure 3.3 Images with different pixel size and the same physical size

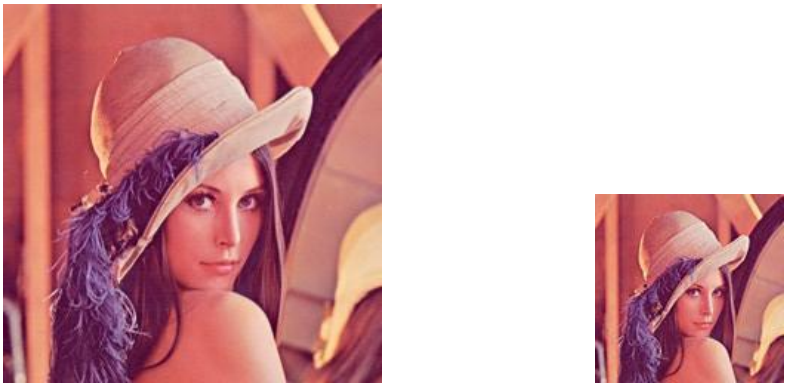

a)Original image (pixels: 256×256) b)Edited image (pixels: 128×128)

Figure 3.4 Images with different pixel size and different physical size

In the proposed imaging system, each receiver array element will represent a pixel in the image where their physical location determines the pixel location. Thus, the signal received by each element will provide the intensity and phase information of the corresponding pixel in the image. In order to obtain a higher quality image two factors should be taken into account first of which is the number of array elements which represents the number of pixels. On the other hand, to obtain a high resolution image, for an object with certain physical size, the spacing between each element should be minimized. However, this will cause mutual coupling (cross talk) between the array elements. This problem imposes a design tradeoff between the resolution of the array and the overall system sensitivity and dynamic range.

To reduce the mutual coupling effect up to a considerable extent, the receiving array elements will be switched on one by one. This is done by connecting array elements to a set of switches that control them. Other than the advantage of cross talk reduction, the switches can provide information about the spatial location of the receiving array element which is useful for image generation. However, the switches cannot eliminate the effect of mutual coupling completely; yet, it can be further reduced by loading each array element. After the scattered signal is received by an antenna element, since it has passed through different mediums, its power is going to be quiet low. To compensate for these power losses, the received signal will be passed through a low noise amplifier. Moreover, this signal is at a very high frequency (10GHz) which requires very high resolution ADC which is quiet expensive. Thus, it will be mixed with the signal from the second port of the directional coupler to bring it down to a baseband signal.

Afterwards, this baseband signal will be fed to the processing unit in which the phase and magnitude components of the image can be separated and shown on the computer.

3.1.1 Antenna designs

As mentioned earlier, one of the most important parts of this design is the receiving antenna (retina). There are two different antennas used in the proposed system one of which is the transmitter antenna (illumination source) and the other one which is one of the most critical parts of the system is the receiver retina. Even though it is not as critical, the transmitting antenna plays an important role in this design. Since the power that can be generated by the signal generator is limited, the transmitting antenna needs to have acceptable radiation properties.

One of the main determining factors in the design of an antenna is its physical size which decides the antennas size, gain and directivity (i.e. as the frequency decreases, its physical size increases, and it can radiate or receive more power). However, the physical diameter of a transmitting antenna determines it’s near field and far field locations (Equation (2.1)).

As for now, the proposed system is to be designed and work in the far field of the transmitting antenna. Since the system is aimed to be as compact as possible, the

transmitting antenna should be as small in size as possible. Thus, there are other characteristics that should be considered in order to maximize the power radiation efficiency. To test different possibilities, for now two different transmitter antennas are going to be studied; a single horn antenna and an array of circular patch antennas.

3.1.1.1. Transmitter

In this work, a horn antenna is used as the transmitter. However, an alternative would be use of an array of circular patch antennas, the design of which is more challenging.

Horn antenna

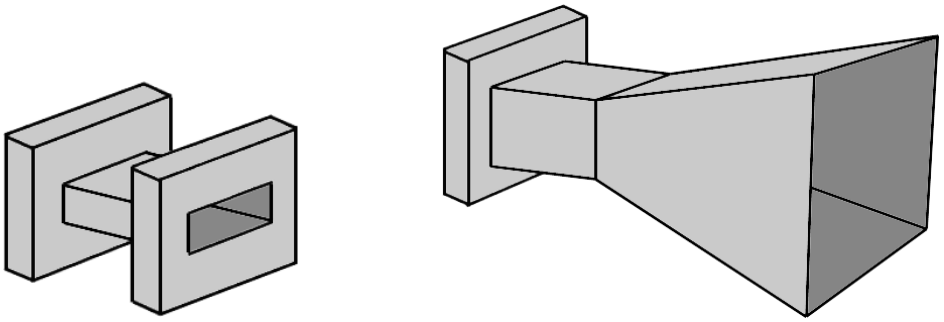

(a) (b)

Figure 3.5 (a) Waveguide (b) Horn antenna

A horn antenna (Figure 3.5) is basically a wave guide with one of its ends flared out. The main function of a horn antenna is to produce a uniform phase front with aperture larger than a waveguide to provide higher directivity, and higher gain (Equation (3.1)).

$$G = e.D \tag{3.1}$$

where,
e is the total efficiency of the antenna,
D is the directivity of the antenna.

The directivity can be further increased by increasing the physical size of the antenna. However, as mentioned before, since the imaging will be done in the far field of the antenna, the dimensions of the antenna are limited. Yet, if a source with higher power was used, the spacing between the transmitter and the object could be longer, thus a bigger antenna could be used.

Even though such a transmitter can be quiet simple, yet if such a single element antenna is used as the transmitter, the array elements of the receiver will not receive the same amount of power when there is no object in between. That is since according to the Friis transmission equation (Equation (3.2)), the power received by the receiving elements is proportional to the inverse of the distance between the transmitter and the receiver.

$$\frac{P_r}{P_t} = \left(\frac{\lambda}{4\pi R}\right)^2 G_{0t} G_{0r} \tag{3.2}$$

Where,

P_t is the transmitted power,

R is the distance between the transmitter and receiver,

G_{0t} and G_{0r} are the transmitter and receiver gains respectively.

This means that the maximum power is transmitted in the forward direction (direct line of sight); thus, the side elements will receive less power than those at the center. The diagram of Figure 3.6 illustrates this issue further.

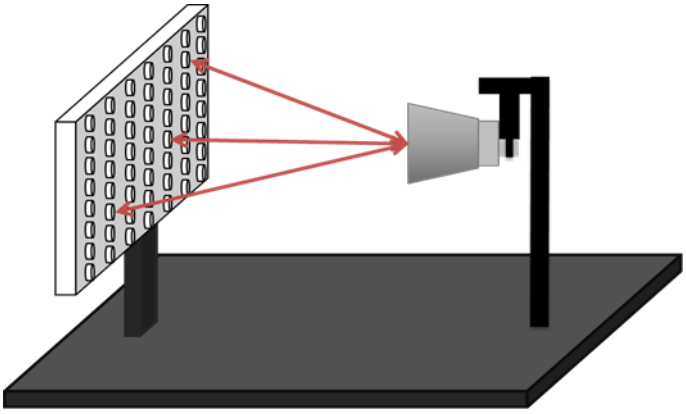

Figure 3.6 Different paths from the transmitter to the receiver elements

Even though this can result in an output that cannot be understood, weight of the array elements can be calibrated to overcome this issue. As mentioned earlier, the power transmitted to the elements far from the center line of the transmitter (the corner elements of the receiver) is going to be small. Thus, if an object with a small skin depth and higher conductivity is to be imaged, its corners will not be illuminated by the system and the image's corners will be vague.

Array of antennas

To overcome such issues, an array of transmitter antennas can be adopted (Figure 3.7). This way, in an ideal mode, each receiving antenna element will receive the same amount of power at all times no matter what the distance between the receiver and the transmitter is.

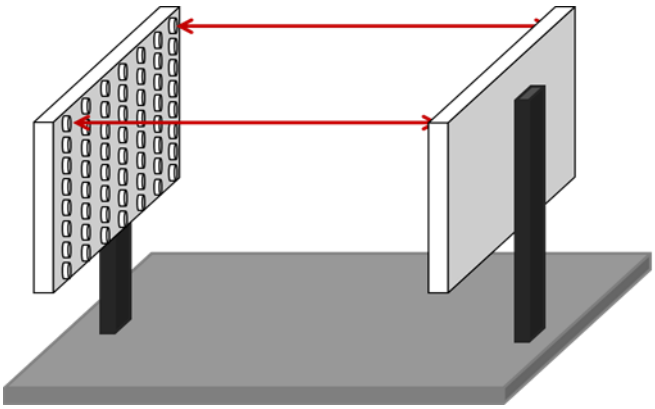

Figure 3.7 Different paths between the transmitter and the receiver when they are similar

Although the transmitted power from each array element is going to behave the same regardless of the spacing between the illumination source and the receiving retina, still there is a need for calibration since in practice, due to manufacturing imperfections, not all of the transmitting and receiving elements are going to be identical. Furthermore, since for the tests only one signal generation source is going to be used, there will be need for switches and cables which are not going to behave exactly the same. This can be fixed by calibration to normalize all the radiated amounts of power from the array elements. Yet, there will be certain drawbacks to such system as well. One of these drawbacks is the complexity and the cost of such a transmitter since it requires many switches and RF cables. Also, the overall radiated power at the transmitter will be less due to losses incorporated with the cables and switches.

Looking into the above mentioned comparison between the two transmitter schemes, it was found that utilization of a horn antenna would be more effective for this prototype since it has a lower cost while it can deliver higher power.

3.1.1.2.Receiver

After an appropriate transmitter is selected, the receiving retina, for which several types of antenna design can be adopted, is to be designed. For this purpose

three different antenna types have been studied and the most appropriate one has been selected. The first type which is the simplest compared to the other elements, is an array of 64 (8 rows and 8 columns) circular patch elements which are small (leading to a higher resolution) and easy to manufacture. The second one is going to be a retina composing of 64 circular slot antennas while the last type will be a 64 element array composing of elliptical resonant slots (in which the array element spacing can be reduced up to a considerable range resulting in a higher resolution). Circular and elliptical slot antenna elements have small physical size and are easy to manufacture as well. Furthermore, if loaded, circular slots can have a considerably high sensitivity at their resonant frequency; yet, the calculations for their design at high frequency are quiet complex and crucial. On the other hand, the elliptical slot antennas have many parameters to be designed for in order to have the desired response. Among all of these types, the circular patch antenna is the simplest to design and manufacture.

Circular patch antenna

Circular patch elements are simply circular conducting planes on a dielectric substrate, and in this case with a minimum spacing of $\lambda/2$ (Figure 3.8).

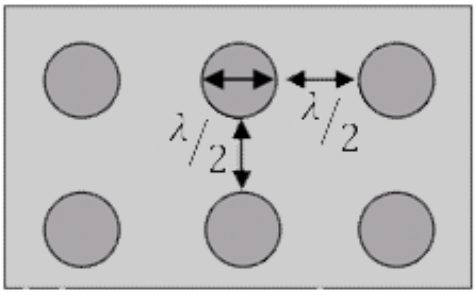

Figure 3.8 Array of 6 circular patched antenna elements

The main factor that should be considered while designing a circular microstrip patch antenna is its radius which can be calculated using Equation (3.3) [29]. This equation can be adopted when the operating frequency and specifications of the substrate (the dielectric permittivity, the dielectric thickness and its loss tangent). Moreover, for this design the antenna is to operate in its dominant mode of TM_{110}.

$$r = \frac{F}{\sqrt{1 + \frac{2h}{\pi\varepsilon_r F}\left[\ln\left(\frac{\pi F}{2h}\right) + 1.7726\right]}} \tag{3.3}$$

Where,

$$F = \frac{8.791 \times 10^9}{f_r\sqrt{\varepsilon_r}}$$

and,

h is the substrate thickness (cm),

ε_r is the substrate permittivity.

Since the system is designed for a frequency of 10 GHz, the substrate was selected to have a loss tangent as low as possible. Thus, RT-Duroid laminate was selected as the substrate material. The parameters of this PCB are listed in Table 3.1.

Table 3.1 Antenna PCB characteristics

Parameters	value
Substrate height	0.787 mm
Dielectric permittivity	2.44
Loss tangent	0.0029
Cladding conductivity	58800 S/mm

Inserting these parameters into Equation (3.3), the physical radius of the circular patch was found to be 0.5099 cm. Even though the main design parameter of the patch is its radius, another important factor, to be considered while designing such an antenna with a coaxial feed point, is the feed location.

Looking at the current and voltage distributions, or the magnetic and electric field distribution respectively, of a single circular patch, it can be found that the current or magnetic field is maximum at the center and minimum near the edges. That is while the voltage or electric field is zero at the center, maximum near the left edge, and minimum near the right edge [30]. This is further illustrated in Figure 3.9.

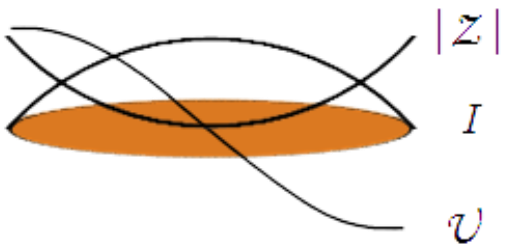

Figure 3.9 Voltage, current and impedance distribution at resonant frequency

From Ohms law, it is known that the impedance and voltage are linearly proportional while the impedance is inversely related to the current. Thus, it can be concluded that the input impedance of the patch is minimum near the center and is maximum near the edges (almost 200 Ω depending on the Q of the leaky cavity). Hence, there is a point where the impedance is 50 Ω along the resonant length at the x-axis of the element.

Mathematically speaking, if the current distribution is known, the impedance can be calculated using Equation (3.5) [31] ,

$$I = \int_s \bar{J}.\overline{ds} \tag{3.4}$$

thus,

$$Z = \frac{2\,P_{total}}{|I|^2} \tag{3.5}$$

where,

J is the current density (A/m^2),

Z is the input impedance (Ω),

P_{total} is the total power received by the antenna (Watts).

Another method that can be adopted to find the feed point is by using Equation (3.6),

$$R_{in(\rho'=\rho_0)} = \frac{1}{G_t}\frac{J_1^2(k\rho_0)}{J_1^2(ka_e)} \tag{3.6}$$

Where,

a_e is the effective radius of the patch,

R_{in} is the input impedance and is known to be 50 Ω,

G_t is the total conductance due to radiation, conduction (ohmic) and dielectric losses.

The effective radius of the patch can be simply found using Equation (3.7) .

$$a_e = r\left\{1 + \frac{2h}{\pi r \epsilon_r}\left[\ln\left(\frac{\pi r}{2h}\right) + 1.7726\right]\right\}^{\frac{1}{2}} \tag{3.7}$$

Also, the total conductance can be found from Equation (3.8).

$$G_t = G_{rad} + G_C + G_d \tag{3.8}$$

Where,

$G_{rad} = \frac{(K_0 a_e)^2}{480} \int_0^{\pi/2} [J_{02}'^2 + \cos^2\theta J_{02}^2] sin\theta \, d\theta$

$G_c = \frac{\epsilon_{m0}\pi(\pi\mu_0 f_r)^{-\frac{3}{2}}}{4h^2\sqrt{\sigma}} [(ka_e)^2 - m^2]$

$G_d = \frac{\epsilon_{m0} \tan\delta}{4\mu_0 h f_r} [(ka_e)^2 - m^2]$

and,

ε_{m0} = 1 for m = 1 (since the mode of operation is TM_{110}),

K_0 is the free space wave number,

After the effective radius and the total conductance are found, the feed point for an input resistance of 50 Ω can be found by iterations using Equation (3.6).

Table 3.2 provides all the parameters calculated for this antenna.

Table 3.2 Calculated parameters of the circular patch antenna

Parameters	The calculated values
radius of the patch	0.5099
effective radius of patch	0.5470
feed location	0.1187

Even though the design and manufacturing of this antenna type is not that complicated, yet there are some drawbacks to this antenna. Since the array elements are conducting materials on a substrate, they will start propagating signals as soon as they are placed in an electric field. The reason is that, as can be seen from Equation (3.9), when a conducting material is exposed to an electric field, current density will start flowing on it

$$J = \sigma E \tag{3.9}$$

where,

J is the current density (A/m^2)
Σ is the conductivity (s/m)
E is the electric field intensity (V/m)

This current density at higher frequencies makes the conducting material to act as an antenna. When placed in a concentrated array, antenna elements will cause interference to their neighboring elements since they start radiating back the signal. This phenomenon is known as crosstalk and can cause a large degradation in the performance of the system especially to the elements located at the center of the array. Basically, crosstalk is the interference caused by two signals becoming partially superimposed on each other due to electromagnetic (inductive) or electrostatic (capacitive) coupling between the conductors carrying signals[20]. A common example of crosstalk is where the magnetic field from alternating current flow in one wire, induces current in another wire running parallel to the other, as in a transformer.

In general, crosstalk can be reduced by using shielded conductors and increasing the distance between them. However, since in this design the aim is to have a reasonably good resolution, the spacing between the array elements has to be as small as possible. A common practice is to place array elements at a minimum spacing of λ/2 from each other. This way, each pixel of the generated image will represent 2.48 cm of the structure under test which can cause a maximum offset of 3.5 cm. Furthermore, the issue of crosstalk can be tackled by using antenna elements that can be loaded such as circular and elliptical resonant slots.

Circular resonant slots

Nowadays, circular resonant slots are potential candidates for the construction of the imaging probes because of their high sensitivity [32]. A circular resonant slot is basically a circular slot in which conducting strips are extended from the ground plane and routed within the slot area such that they add an appropriate capacitive load to the inductive circular slot[32]. However, as mentioned earlier, due to the requirement for high resolution system, the arrays elements are to be close to each other which results in mutual coupling. This issue can be tackled by loading an inductive circular slot by

a capacitive load [33]. To do so, a gap is introduced between the conducting strips the change of which can control the capacitance of it for thin ground planes. As the gap length increases, the resonant frequency of the slot decreases and vice versa. If the slot diameter is chosen to be λ/4 and the gap length is selected 0.46 mm, the slot is expected to resonate around the center of the X-band frequency range (8.2-12.4 GHz)[33]. Figure 3.10 represents an image of an array of two circular slots with spacing D = 34mm.

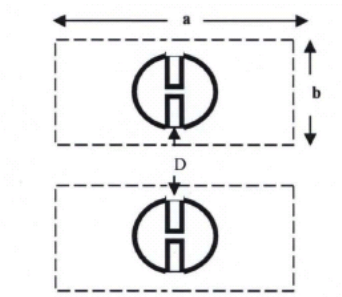

Figure 3.10 Circular resonant slot with capacitive load

Yet, the spacing between each element is considerably large. If such antennas were to be adopted for the receiver, the retina would have looked like Figure 3.11.

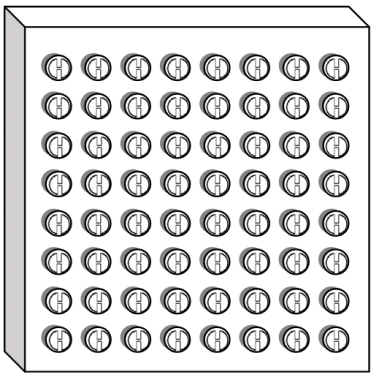

Figure 3.11 Array of 64 circular resonant slots

Even though the circular loaded slots can help in the reduction of cross talk, yet there are other types of antennas that can be adopted for this purpose and provide lower coupling.

Elliptical resonant slot

The other type of antenna that can be used for the array design is elliptical slot antenna. As mentioned earlier, designing such antennas requires lots of calculations and their manufacturing is relatively harder. However, designing this antenna can result in having the switching action integrated with the antenna elements, resulting in cost reduction. Moreover, it reduces the mutual coupling up to a considerable extend.

Basically, as can be seen from the snapshot of Figure 3.12 an elliptical slot is composed of PCB with an ellipse etched on it.

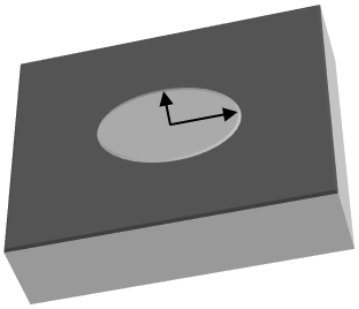

Figure 3.12 Elliptical resonant slot antenna

The main dimensions of this slot can be found from Equation (3.10) given that the frequency of operation is known.

$$f = \frac{30 \times 0.32}{2A + 0.25B} \tag{3.10}$$

where,

A and B are the major and minor radiuses of the ellipse respectively.

Now, to load an elliptical slot, a circular or even an elliptical patch can be mounted inside the iris (opening) of the antenna (Figure 3.13). Afterwards, a PIN diode can be used to either activate that antenna element or deactivate it. The antenna element with the diode in its reverse biased mode will be activated and those with forward biased mode will be inactive.

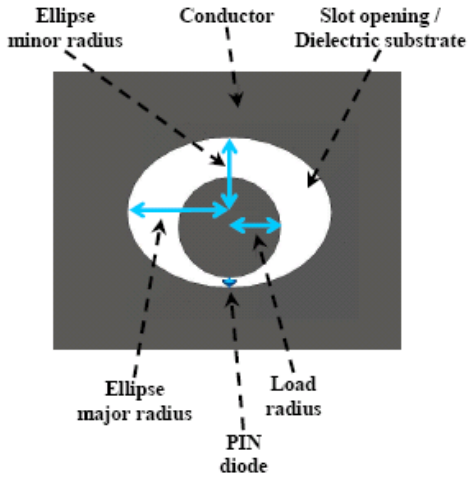

Figure 3.13 Circular patch loaded elliptical resonant slot antenna [16]

This can result in the array elements with their diodes forward biased to be deactivated and most of the current flowing on them will be grounded and only a small amount of signal will reflect from each element.

Even though the loaded circular and elliptic slots can provide a better performance in terms of mutual coupling, yet their design and manufacturing process is more challenging than those of the circular patch antenna. Thus, for the first prototype of this work, the circular patch antenna will be designed and tested. However, as for the later improvements, design of the introduced slot antennas can improve the performance and efficiency of the system up to a considerable extent.

3.1.2 Switching network

Since each antenna element refers to a pixel of the image to be generated, its location is significant. Thus, utilization of a switching network with the circular patch antenna (Figure 3.14) can help finding the address of the each array element. Even though adopting switches can reduce cross talk between antenna elements by selecting one antenna element at a time, yet the designed switches can cause crosstalk in their circuitry.

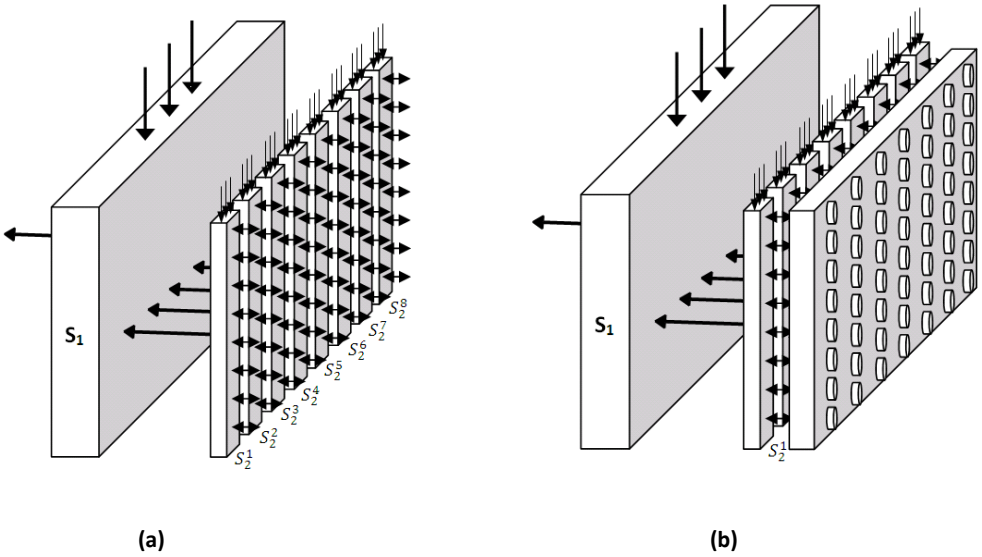

Figure 3.14 The switches configuration (a) without antenna array (b) with antenna array

Different designs can be adopted for the switching network the simplest of which is utilization of an SP64 matrix switch (Figure 3.15). Such a switching network can provide significant isolation of up to 60 dB and a considerably low insertion loss of up to 0.4 dB.

Figure 3.15 Matrix switch

Even though, such switching networks can enhance the performance of the overall system by providing high isolation and low insertion loss, yet they are quiet expensive and bulky. Another switch design that can be adopted is connectorized SP8T (single pole, 8 through) switches which are a switch module with SMA connectors (Figure 3.16). Even though these switches have acceptable characteristics and are cheaper than the matrix switches, yet they are expensive. The other drawback

related to these switches is the losses that they add to the system due to external cables used for connecting them. That is since the antenna has 64 elements and 9 SP8T switches are required (Figure 3.14a). Eight of the switches are used for antenna elements connections and one is used for connecting the switches together. These additional losses that are due to reflections at the SMA connectors and the others are due to the losses in the cables themselves.

Figure 3.16 SP8T switch module

However, other than adopting loaded elliptical resonant slot antennas with PIN diodes, there are other alternative techniques that can be considered in order to improve the switching network. One of these alternatives is designing a switching network that has IC switches (Figure 3.17) interconnected to each other on a PCB. These switches are much cheaper than the external switches (by a factor of up to 100 depending on their type) and the size of such a network can be smaller than that of Figure 3.16. However, there are certain issues with this method such as its complicated PCB design which is quiet challenging and its manufacturability which cannot be done locally. That is since at such high frequencies every single part should be designed and manufactured with special considerations.

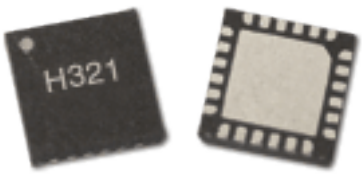

Figure 3.17 SP8T IC switches

3.1.2.1. Switching network design

The switches selected to be used for this design were HMC321LP4E switches manufactured by Hittite, an outline of which is shown in Figure 3.18. These are broadband non reflective GaAs MESFET SP8T switches in low cost leadless surface mount packages. These switches offer high isolation and low insertion loss and they include an on board binary decoder circuit which reduces the required logic control lines to three for each. They operate using a positive control voltage of 0/+5 volts, and require a fixed bias of +5v. Moreover, they are suitable for use with 50ohm transmission lines. However, this switch operates best in the frequency range DC-8 GHz. Yet, it has an acceptable performance for prototype testing at 10 GHz.

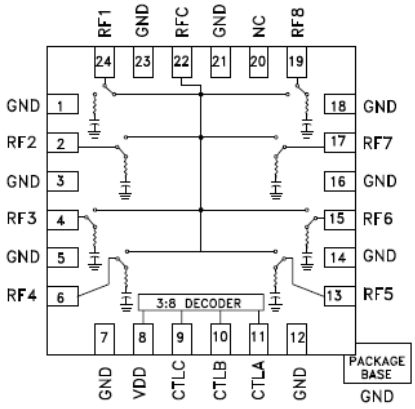

Figure 3.18 SP8T HMC321LP4E switch

One of the main considerations to be taken into account for these switches is utilization of a bypass capacitor in order to remove the DC part of the signal coming out of the switches. To do so, 100 pF capacitors were used in series with each switch port (Figure 3.19).

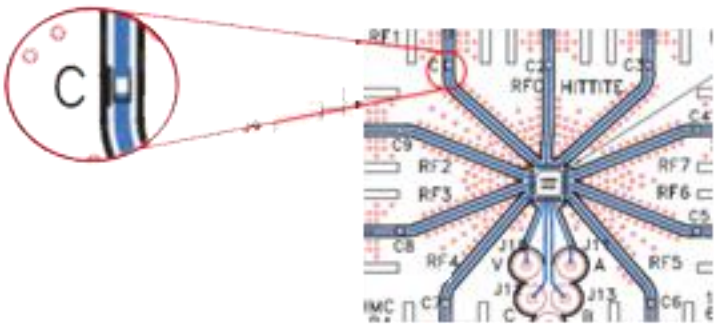

Figure 3.19 PCB mounted test switch with capacitors

Other components required for the switching network are SMA connectors which are used as an interface between the switches. Even though the cable connecting the antenna elements to switches could be soldered to the switch PCB, yet there are some drawbacks to this configuration. The first issue is that if some fault happens in the switching network and one of the components is required to be replaced, the cables will make the maintenance process difficult. Also, the switching network will be attached to the system and it can only be used for this system. The SMA connectors used for this purpose are Emerson's microwave Jack SMAs (Figure 3.20).

Figure 3.20 SMA jack connector

After the components were chosen, the main part was PCB lamination selection. Since the system is to work at microwave frequencies, the lamination that was selected had to have a very low loss tangent (i.e. had to be low loss laminate). Other than the lamination material, the board's thickness and the copper cladding of the board (which is referred to as the copper layer of the PCB) had to be selected based on certain considerations (Figure 3.21).

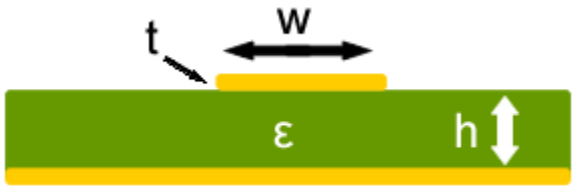

Figure 3.21 PCB with strip line

These can be determined by some constraints considered for the layout and the overall systems; such as the characteristic impedance of the tracks, the size of the switches pads and the system's frequency of operation. Since the components acquired for the system had a characteristic impedance of 50 Ω, the tracks widths had to be calculated such that their impedance is 50 Ω to minimize the mismatch losses. This width can be calculated from Equation (3.11) [11].

$$\frac{W}{h} = \begin{cases} \dfrac{8e^{A}}{e^{2A}-2} & for\ \dfrac{W}{h} < 2 \\ \dfrac{2}{\pi}\left[B - 1 - \ln(2B-1) + \dfrac{\varepsilon_r - 1}{2\varepsilon_r}\left\{\ln(B-1) + 0.39 - \dfrac{0.61}{\varepsilon_r}\right\}\right] & for\ \dfrac{W}{h} > 2 \end{cases} \tag{3.11}$$

where,

h is the board thickness,

$$A = \frac{Z_0}{60}\sqrt{\frac{\varepsilon_r + 1}{2}} + \frac{\varepsilon_r - 1}{\varepsilon_r + 1}\left(0.23 + \frac{0.11}{\varepsilon_r}\right),$$

$$B = \frac{377\pi}{2Z_0\sqrt{\varepsilon_r}}$$

As can be seen from Equation (3.11) the width of the transmission line is directly proportional to the height of the board. On the other hand, it is inversely proportional to the lamination's dielectric permittivity. Thus, these parameters have to be selected in such a way to meet both the availability of the materials in the market and minimize losses due to changes in the size of the tracks (i.e. the track widths should be close to the size of the switches pads so that the change in the size of tracks is minimized).

Moreover, the width of the tracks cannot exceed a certain number since at a certain track width; the track can act as a radiator with a high radiation efficiency

which can cause a huge degradation in the level of signal that goes out of the switches. This width can be found from Equation (3.12)[29].

$$W = \frac{1}{2f_r\sqrt{\mu_0\epsilon_0}}\sqrt{\frac{2}{\epsilon_r + 1}} \tag{3.12}$$

After all the calculations and considerations, it was decided to select Rogers 4003 with the characteristics mentioned in Table 3.3.

Table 3.3 Switch PCB Characteristics

Parameters	
Dielectric permittivity	3.55
Lamination thickness	0.031”
Copper cladding	1 Oz
Loss tangent	0.0029

Applying the data provided in Table 3.3 and noting that the frequency of operation is 10 GHz, a track width of 1.7435 mm was found for the switches. A snapshot of the overall layout of a SP64T switch designed for this work is shown in Figure 3.22. However, when it came to manufacturing, it was found that such a switching scheme cannot be adopted for the initial tests and it can be used for the finalized prototype on the future. One of the main issues was that in the prototype test phase, it can be quiet challenging to follow the possible faults in the network.

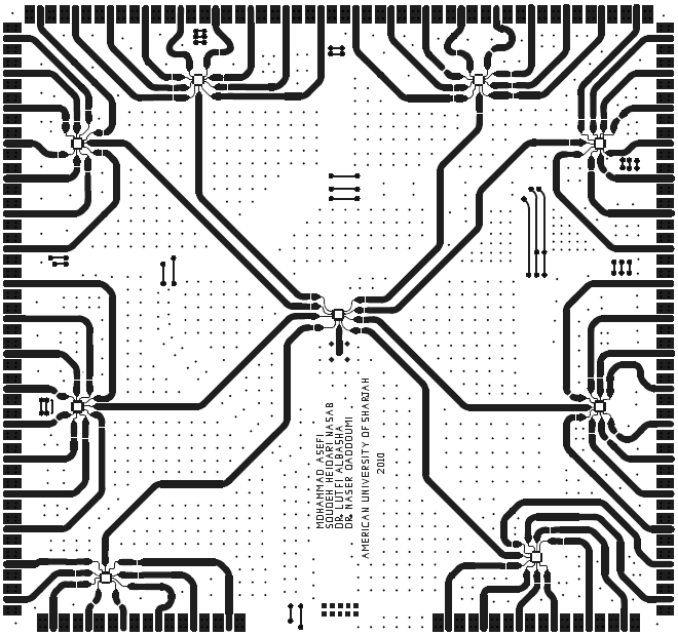

Figure 3.22 Designed SP64T switch layout

Figure 3.23 represents a snapshot from the layout of the SP8T switch. One of the main benefits of this switch over the SP64T is that if a switch is not working properly it can easily be detected and replaced. However, the external cables that are used in this scheme are more in number and this causes some degradation in the power of the received signal.

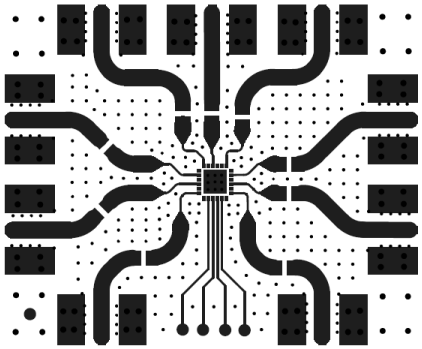

Figure 3.23 Designed SP8T switch layout

As can be seen from both layouts, the signal lines have been tapered in order to reduce the reflection and mismatch losses due to different sizes of the 50 Ω track widths and switches pads.

As mentioned earlier, since there are 64 antenna elements on the array, 9 SP8T switches are required and the output of the ninth switch is to be connected an IQ mixer.

3.1.3 Mixer

The signal received from the antenna is at a very high frequency and it needs to be down converted using a mixer. However, if a normal mixer is used, the down converted signal will only provide the magnitude information of the image obtained for the object/structure while an image is composed of two parts; magnitude and phase. Moreover, a considerable amount of information about an image is in its phase. In order to extract both magnitude and phase information of the image, an IQ mixer will be used. This way, the received signal gets divided into two parts. One of them gets mixed with the local oscillator signal that was generated earlier while the other gets mixed with the same signal having a 90° phase shift so that a complex dc signal can be obtained (Figure 3.24).

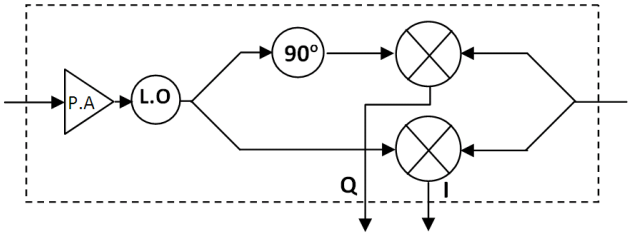

Figure 3.24 The down conversion unit

As for the local oscillator, the signal that was extracted from the signal generator via the directional coupler is used so that the information signal can be directly down converted to DC. However, this signal is very low since most of the original signal is delivered to the transmitting antenna. Thus, it will first get amplified through a power amplifier. The signal at the output of the power amplifier needs to have a minimum power of 10 dBm. After this stage, the signal will be fed to a computer for processing and analysis.

3.2 The imaging system software

When a signal hits the SUT and gets reflected, its reflection goes through certain hardware as explained earlier. However, this signal requires a processing unit to analyze it and after certain operations produce an image of the SUT. To do so, the collected data from each array element will be taken to MATLAB for processing through a National Instrument data acquisition card (NI-DAQ). The MATLAB code will have two parts, one of which will be data collection and switch activation while the other part will be image processing. The later part is just to enhance the quality of the image obtained from the camera.

3.2.1 Switching

Before any data can be collected, the antenna elements on the retina have to be activated one by one so that their location can be stored. Since the system is aimed to provide a pseudo-real-time view of the structure under test, the main concern of this part will be writing a code by which the time and method of switching is optimized. One of the factors that can further improve the switching scheme is the use of two IQ mixers rather than one. That is since at each instance two of the array elements are activated and the time required for scanning the whole array will be reduced to 50%.

At this stage the acquired data will be stored in a matrix the elements of which represent the location of the elements on the retina and their value corresponds to the intensity of the image. That is since each array element corresponds to a pixel of the image to be obtained.

3.2.2 Image processing

As soon as the image matrix is obtained, it will be normalized to compensate for the possible differences in the maximum power level received by each array element. Later, the data will be mapped to a Jet coloring scheme to provide a reasonable visual realization of the image. At the end, an image will be graphed which gets updated every few seconds.

CHAPTER 4

FABRICATION AND MEASUREMENTS

The first section of this chapter provides a description of the manufacturing of the proposed microwave imaging system. An overview on how the antenna array was fabricated and developed is presented. The first section presents the overall system and the possible sources of errors. As for the second section, solutions to compensate for such errors are provided. In this section, the calibration of the overall system is also explained in detail. Furthermore, this section includes some of the challenges during the calibration process. This chapter closes with a section on practical tests, ran to investigate the performance of the proposed microwave imaging system.

4.1 Fabrication

As mentioned earlier, the hardware of the proposed imaging system includes three main parts; the antennas, switching network, and the down conversion unit. As for the down conversion unit, an IQ mixer was selected to be used. That is while the other two sections had to be designed and fabricated according to the needs.

4.1.1 Antenna fabrication

After the dimensions of the elements were calculated accurately as explained earlier, they were taken to be printed on a PCB for which there were two different options. One of them was using an automatic PCB printing machine which uses routing and drilling bits to process PCBs. One of the main advantages of this machine is that it can print layout routs at their accurate locations at one step. However, since it uses routing bits, it could introduce some sharp and unsmooth edges. At high

frequencies, these edges can cause radiations which cannot be tolerated in the proposed system due to small spacing between array elements. Moreover, the routing bits can scratch some parts of the dielectric substrate which can cause non-uniform distribution of the electric field on the array elements.

The other option that could be adopted for PCB printing was the use of a chemical process. Even though this process could eliminate sharp edges up to a considerable extent, it requires proper masking during the UV exposure and timing during the PCB development and etching phase. Despite such issues and after some tests, the chemical process was found to be more suitable for printing the antennas.

Afterwards, the coaxial feeds had to be soldered to array elements. One of the main considerations during this part of the process was the fact that no space had to be left between the ground plane at the back of the retina and the insulator of the coaxial cable. That is since it can cause a disturbance in the electric field and some part of the signal would radiate. Furthermore, the feed line (the wire at the centre of the coax) could touch the ground plane and cause unreasonable results. Figure 4.1 illustrates this effect.

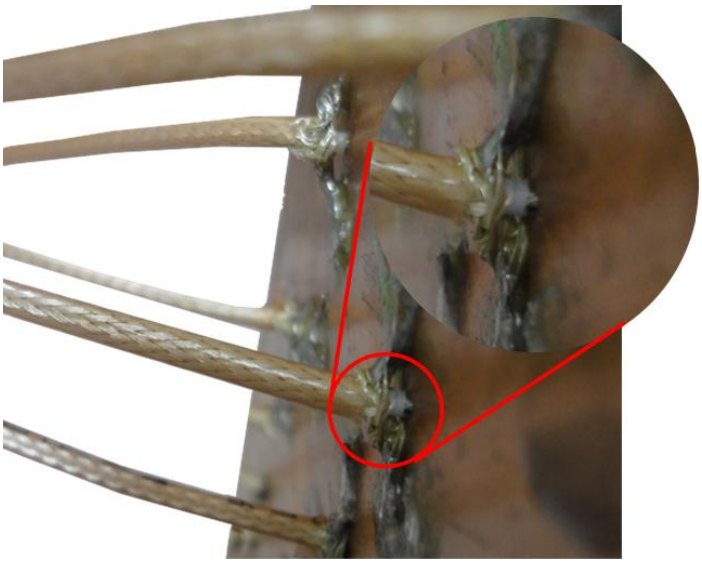

Figure 4.1 Improper cable soldering

Later on, a stand was designed and fabricated to hold the receiver and transmitter antennas. The main consideration about the stand was its material which was decided to be epoxy glass since it could not be of anything with conductivity.

4.1.2 Switch network

After the switches were designed and fabricated, the components were mounted on them. Figure 4.2 provides a snapshot of one of these switches.

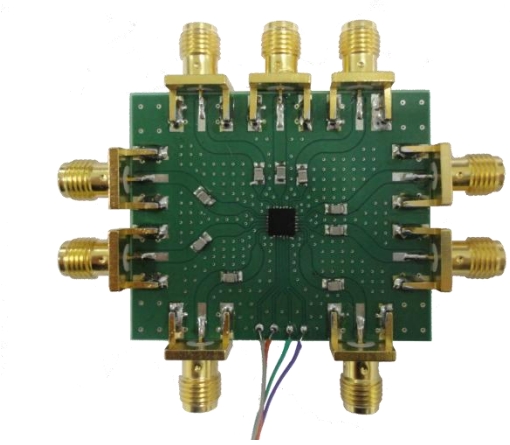

Figure 4.2 SP8T switch

The performance of the switches can be tested either by a vector network analyzer or by inputting a signal of certain frequency and power at the pole port and measuring the output at the through ports. Since a vector network analyzer with frequency of operation of up to 10 GHz did not exist at the labs, the second method was adopted. Thus, a microwave signal with a power of 5 dBm at 10 GHz was applied to the pole port of the switch and the output at other ports was observed and it was found that the switches introduce an attenuation of almost 5 dB to the input signal. Furthermore, the leakage from each port was found by inputting the signal to one of the ports and measuring the output at the other ports. And, it was found that all the ports had a negligible leakage while the first port had a considerable leakage that could affect other ports while it was not activated.

4.2 System Calibration

Generally, calibration is known as the act of checking or adjusting the accuracy of a measuring instrument. As for this project, calibration is required to unify the effects of all the array elements at the output of the final switch. There are several reasons for the array elements to have different responses one of which is their soldering. As can be seen from the snapshot of Figure 4.3, the feed of each array element is soldered different from the others since they are hand soldered. For some elements the soldering is better while for others it has some flows.

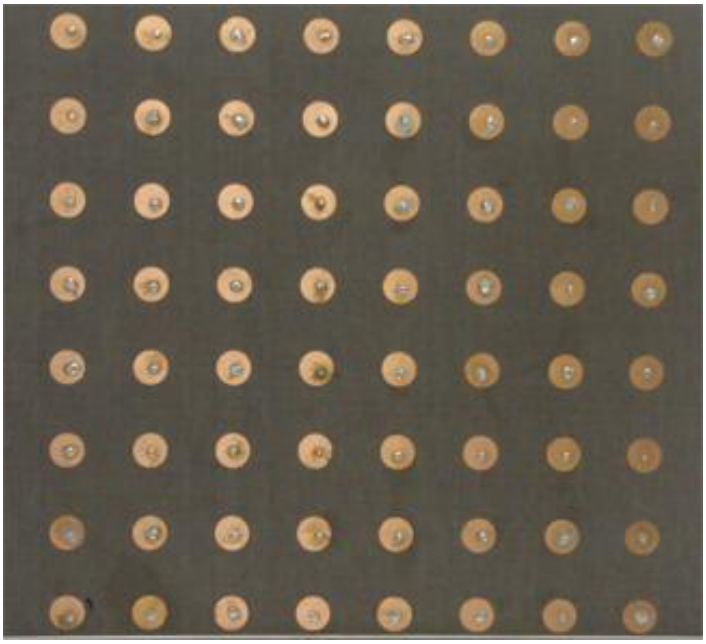

Figure 4.3 64 element retina

The other factor that can cause array elements responses to vary is the length of cables connecting each array element to the first row of switches. Even though the cables are tried to have all the same sizes, yet some of them are shorter than the others. Furthermore, since the switch connectors are also hand soldered, each of them might have a different response. Other than these human errors, there is another main part of the system that causes this non-uniformity of array element responses and that is having a single element transmitter. Even if all other issues were negligible, the effect of the radiation pattern of the transmitter and its transmitted power to each element had to be calibrated. As shown in Figure 3.6, the power received by each array element varies due to their location with respect to the transmitting antenna.

The calibration process can be done once when the system starts up if the location of either the receiver or the transmitter and the amount of transmitted power are not changed. Otherwise, the calibration must be done whenever a change takes place. Moreover, whenever the surrounding environment of the system changes, i.e. if something gets located or removed from the area around the system that did not or did exist during calibration, a calibration is required. Thus, to make the system more reliable, each time the system is switched on and is ran for the first time, it automatically gets calibrated.

In order to calibrate the system, first any object between the transmitter and the receiver has to be removed. Afterwards, a signal should be radiated from the

source to hit the receiving retina and the signal captured by each antenna element will be recorded. These values will be the reference weights that when divided by a received signal with an SUT in between, normalized values will be obtained. Afterwards, these normalized values with respect to the maximum power that each element can receive, can be adopted to accurately analyze the SUT. The images obtained from the system before calibration (the reference image) and after calibration are shown in the snapshots of Figure 4.4 (a) and (b) respectively.

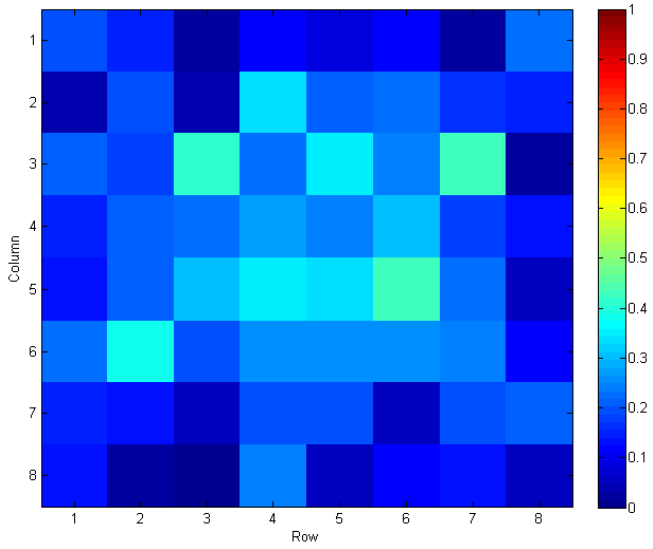

(a)

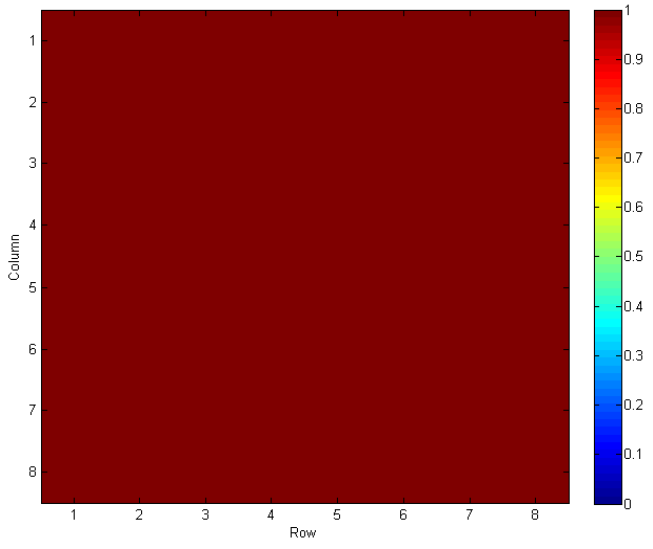

(b)

Figure 4.4 Snapshot of the received signal before (a) and after (b) calibration

4.2.1 Range grouping technique

Even though the calibration process looks simple, there were some challenges the main one of which was the varying power generated from the sweep oscillator available in the lab. Since the images obtained using this system are mainly based on the reflected signal intensity level variations due to existence of an object between the source and the receiver, any small variation of the generated signal would cause a miscalculation. However, since the variations were not severe, a decrease in the sensitivity of the system by rounding the measured data to an accuracy of 1/100 could solve possible faults caused from this source of error. Yet, this was at the expense of less sensitivity to objects with dielectric characteristics close to that of the air.

The same technique could be approached differently by rounding the normalized values within certain range to a specific value. This can help elimination of small power variations. At the same time, it can cause the signal power variations due to objects with dielectric characteristics close to that of air to be ignored. This can be done by the MATLAB code provided in part a of Appendix A.

4.2.2 Real time microwave generator variation feedback

A better solution for elimination of the generator power variations would however be the use of a real time calibration with a feedback from the power generation unit. This can be done by monitoring the power variations of the generated power using a diode detector. The output of this detector would be fed to the MATLAB via the data acquisition card. Before a signal is measured from each array element, first the generated power is measured. If the power is the same as that of the first calibration, the system gathers the required data with the previous calibration. However, if the generated power is changed, the variation percentage will be calculated and the corresponding element in the reference matrix will be increased or decreased with the same percentage. Even though this technique increases the data acquisition and thus the imaging time; yet, it can provide a considerably enhanced image of the SUT. However, other than the increase in data acquisition and processing time, adoption of this technique increases the costs of system. That is since additional components such as coupler, power amplifier, diode detector and cables would be required. The proposed MATLAB code for this operation is provided in part b of Appendix A.

Among all, the technique adopted for reduction of the generated power variations was the normalized matrix rounding technique since it required no additional components. Furthermore, for system tests, structures/objects with dielectric characteristics higher than that of air were used. Thus, rounding of small power variations would not have any significant effect on the system performance.

4.3 Practical Tests and Results

After the system was calibrated, an object of certain shape was placed between the two antennas (transmitter and receiver). The main consideration at this point is to place the object in the far-field of the transmitter which is obtained from Equation (2.1) and is found to be 4.2 cm from the transmitter.

The first test was to detect an object inside a dielectric structure. To do so, an aluminum foil made to the shape of a gun (Figure 4.5 (a)) was placed inside a Styrofoam (polystyrene) cube as shown in Figure 4.5 (b).

(a)

(b)

Figure 4.5 An aluminum foil gun (a) inside a Styrofoam cube (b)

Afterwards, the object was placed between the transmitter and the receiver (Figure 4.6). As mentioned earlier, the main consideration at this point would be the spacing between the transmitter and the object to be imaged (which is a minimum of 4.2 cm from the transmitter antenna.

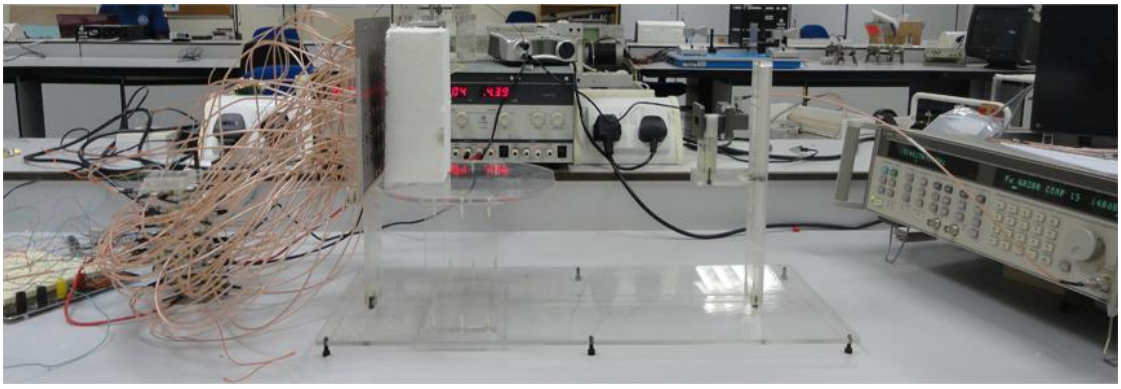

Figure 4.6 Snapshot of the test setup

To measure the performance of the system, first a 12dB microwave signal at 10.1 GHz was generated and radiated from the transmitting antenna. To obtain the image of the object in the Styrofoam, first the system was calibrated as explained earlier. Afterwards, the cube's location was altered so that the proper layer of the Styrofoam, where the gun was hidden, could be scanned. At the end, by running the code presented in Appendix A, a 64 (8×8) pixel image was obtained. Figure 4.7 (a) represents a snapshot of this image.

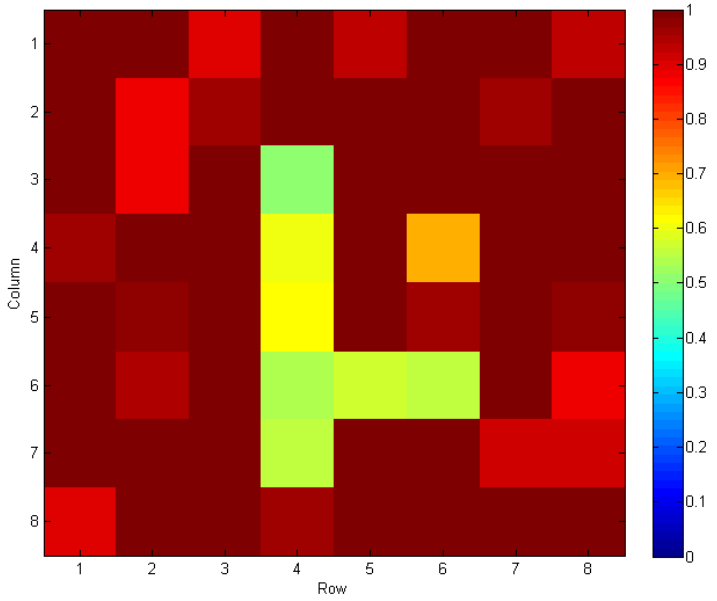

(a)

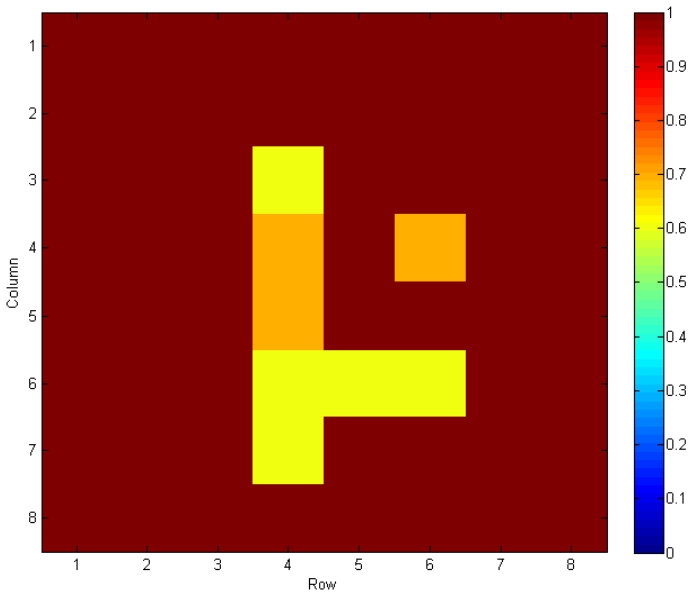

(b)

Figure 4.7 Image of object inside Styrofoam before (a) and after (b) range grouping (64 pixels)

As can be seen from the image of Figure 4.7 (a), there are many power variations at most of the pixels which reduce the visual quality of the image. However, applying the technique of range grouping, as explained in previous section, to the image, a more visually appealing image can be obtained (Figure 4.7 (b)).

Even though the image presented in Figure 4.7 (b) provides a reasonable approximation of the object of Figure 4.5 (a); yet, it does not include all the details of the object. That is since the array elements are not enough for representing a fine image of the object under test. Moreover, information about the parts of the object that are within the spacing between the antenna elements is lost. Additionally, as can be seen from the obtained results, the largest dimension of the image is represented by 5 pixels. This means, that the vertical size of the image is 12.4 cm which is 1.4 cm larger than the actual value and results in 11.8 % difference. As for the other dimension of the imaged object, the percentage difference is found to be 21%.

However, these errors can be reduced either by increasing the array elements and decreasing their spacing, or imaging an object several times, each time with a slight horizontal or vertical shift. Then the images can be superimposed on each other to provide a higher resolution image of the object. Even though the first method can enhance the performance of the system, yet at this stage of work it is not possible due to lack of resources. That is while the second method can enhance the obtained image

at the cost of the image processing time. That is since only separate images of the object can be taken and after a few trials, an overall image of the whole object can be presented. Figure 4.8 (a) and (b) represent a 128 pixel (8×16) image of the object of Figure 4.5(a) before and after range grouping respectively.

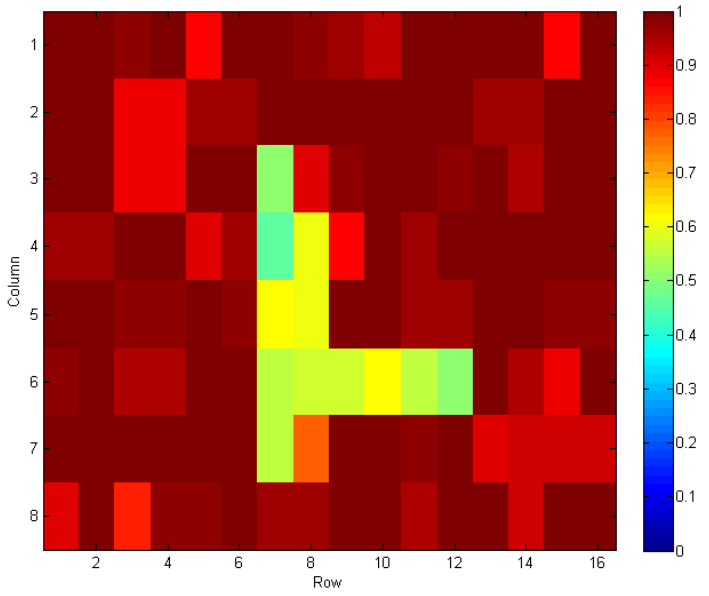

(a)

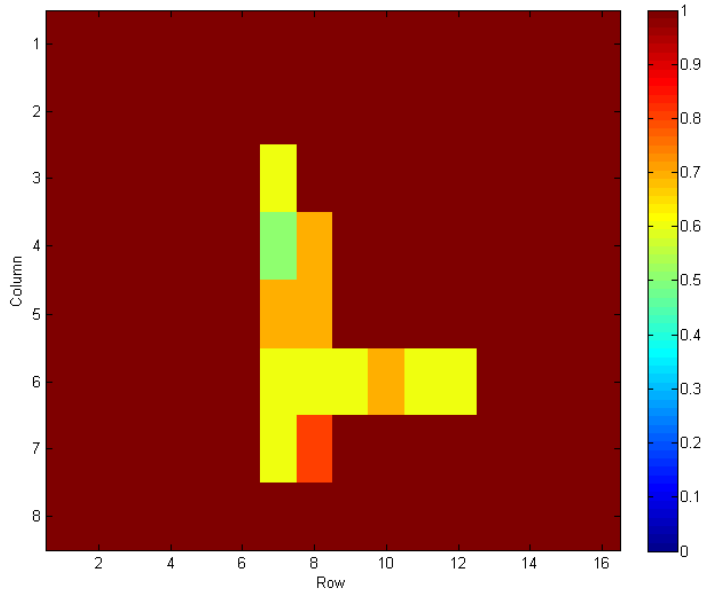

(b)

Figure 4.8 Image of object inside Styrofoam before (a) and after (b) range grouping (128 pixels)

As can be seen, this image provides a more detailed representation of the object. Later on, to test the system further with a different setup, the Styrofoam cube

was placed in front of the retina with an angle (Figure 4.9(a)) for which the image of Figure 4.9(b) was obtained.

(a)

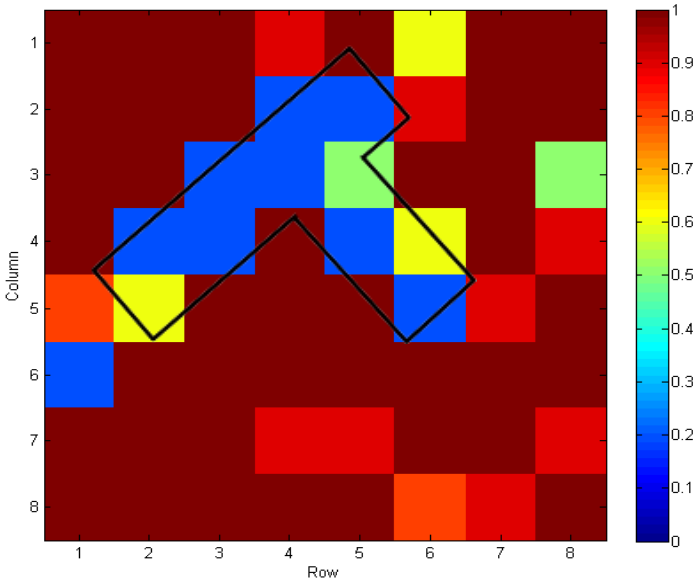

(b)

Figure 4.9 (a) The configuration of the object in front of the retina and (b) The image of the object

Even though there are many erroneous pixels, yet the image of the gun is somehow visual. For further investigation of the performance of the proposed imaging system, object of Figure 4.10 (a), which is a 15 cm plastic pen, was placed in front of the retina. For this configuration, image of Figure 4.10(b) was obtained. As can be seen from the image, the pen is completely visible. Moreover, it can be viewed that the intensity of pixels due to presence of a plastic material is lower compared to the aluminum foil.

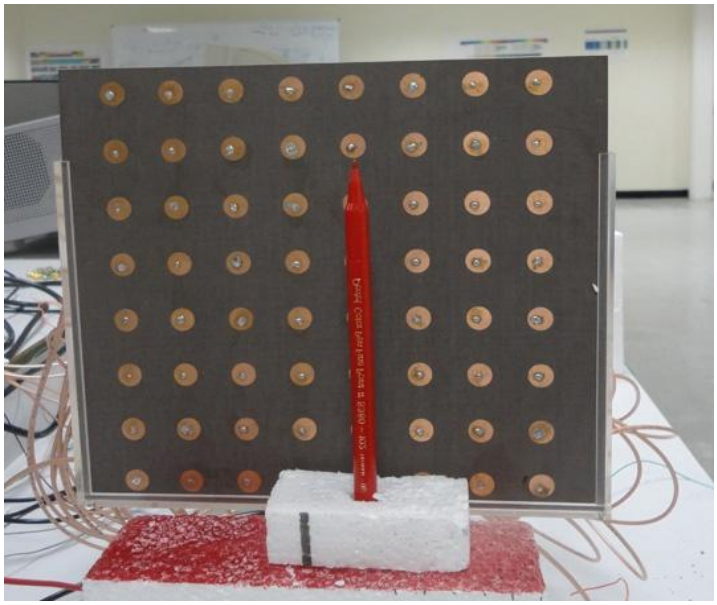

(a)

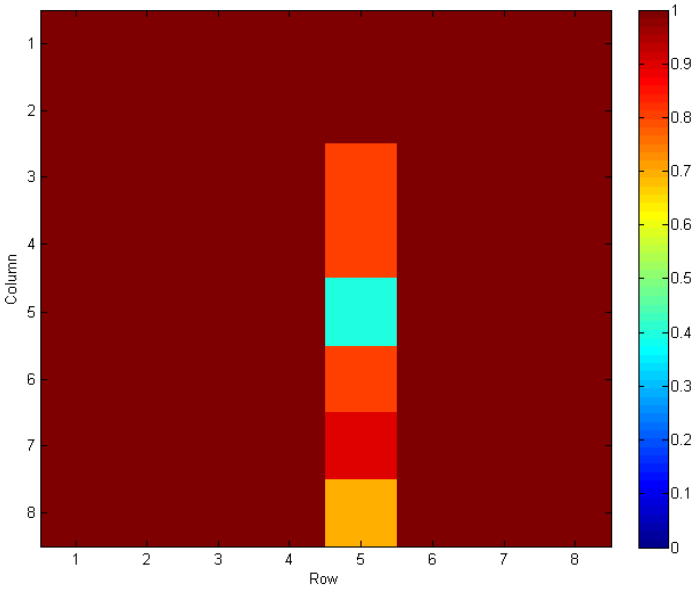

(b)

Figure 4.10 Plastic pen (a) and its image (b)

As can be observed from this image, the size of the imaged pen is 15 cm which is exactly the same as the actual size. Later on, a 6 cm by 2.2 cm hexagon wrench (Figure 4.11 (a)) with a thickness of 3 mm and a metallic rod (Figure 4.11(b)), with a height and thickness of 4.5 cm and 4 mm respectively, were hidden in a Styrofoam and imaged separately. Figure 4.12 (a) and (b) represent the images obtained from scanning these two objects respectively.

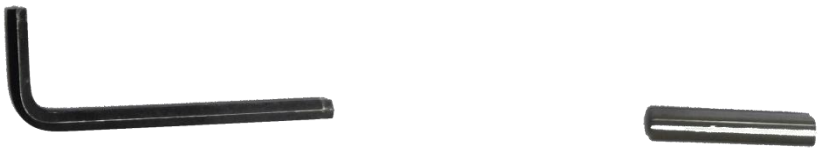

(a) (b)

Figure 4.11 (a) Hexagon wrench and (b) metallic rod

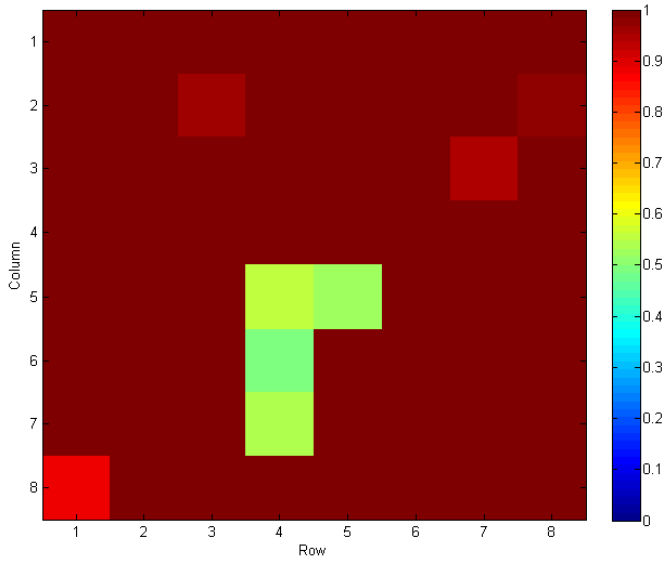

(a)

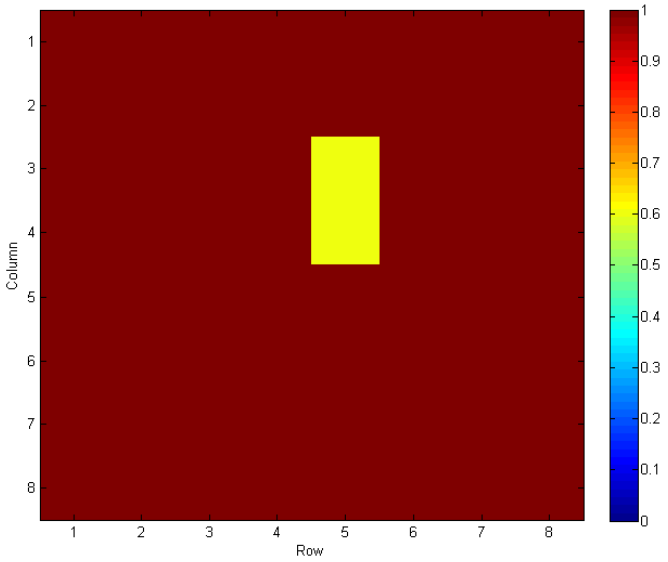

(b)

Figure 4.12 Image of the hexagon wrench (a) and metallic rod (b)

From Figure 4.12(a) and (b), it can be observed that the shape of the objects is completely visible. However, as for their sizes, the hexagonal wrench has a 15% difference in its height and 70% difference in its width. That is while the metallic rod

had a percentage difference of 10.5% in its height. As mentioned earlier, these errors can be reduced by increasing the resolution of the imaging system. By doing so, when the horizontal resolution of the imaging system was increased to 16, the percentage error for the horizontal arm of the wrench was decreased to 14%.

At the end, to test the sensitivity of the proposed imaging system to different materials, a metallic, wooden and plastic rod were located in a Styrofoam and imaged at the same time. Figure 4.13 shows the image obtained from this test. As can be observed, each material is presented by different shades of colors resulted by their structural material (or dielectric properties).

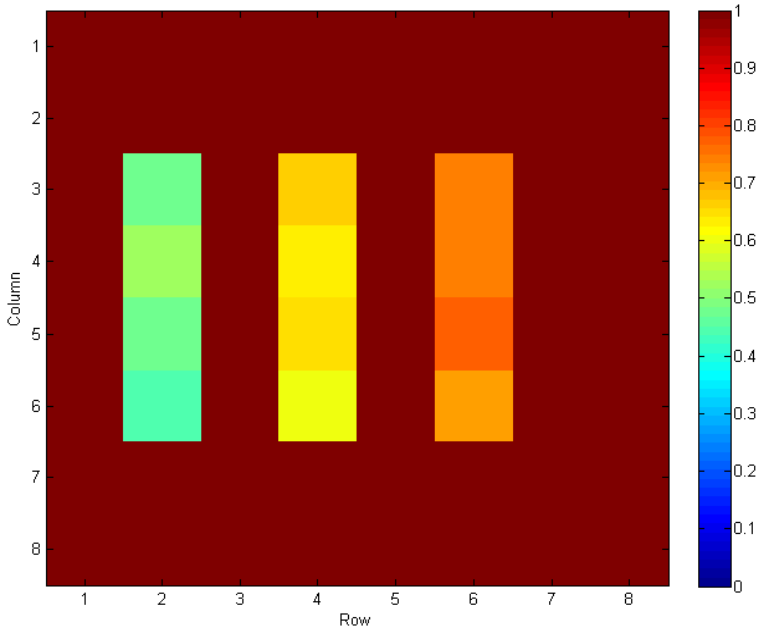

Figure 4.13 From left to right, are the images of the metallic, wooden and the plastic rods

CHAPTER 5

CONCLUSIONS AND FUTURE WORK

5.1 Conclusions

This research has provided a new solution to the problem of pseudo real time imaging. This can be the base for further research to develop a pseudo real time microwave imaging system. During the research, plenty of observations, the main ones of which are going to be summarized in this section, were made at each stage of work.

One of the achievements of this thesis was high frequency switches designed and fabricated in the labs. Even though such switches can be found easily in the market, yet the designed switches were quiet cheaper with almost similar performance. The performance of these switches could be increased considerably by utilizing PCB substrate with higher dielectric permittivity and lower loss tangent. It is worth to mention that such PCBs were not used due to lack of time and their availability in the market.

Another achievement of this project was its capability to provide real time images with a refresh rate of less than ten seconds. Yet, for testing purpose and due to lack of a stable signal generator, this refresh rate was increased to almost thirty seconds to increase the sampling period and thus the accuracy of the image. However, if a faster data acquisition card was utilized, this timing could be further reduced.

5.2 Recommendations for Future Work

There are some improvements that can enhance the performance of the microwave camera. The main improvement to the system is alteration of the receiver antenna array. A loaded circular or elliptical patch, as mentioned before, array can

provide a better performance. Furthermore, if PIN diodes are used to modulate the received signal, the switch network can be eliminated.

As explained earlier, this camera can be adopted to image different layers of the structure under test. However, at this stage, the focusing effect with which layers of the SUT could be scanned one by one is not explored and is left for the future developments.

Moreover, another part of the proposed system that can be enhanced is its switch network. A more compact switch network (or switch matrix) with higher isolation (lower coupling) and less attenuation can improve the performance of the proposed system considerably.

Even though these improvements can enhance the accuracy and visual quality of the obtained image, yet the overall concept of the system will remain almost the same as the system presented in this thesis.

REFERENCE LIST

[1] N.-E. Belhadj-Tahar, A. Fourrier-Lamar and H. de Chanterac, Broad band simultaneous measurement of complex permittivity and permuability using a coaxial discontinuity, IEEE Trans Microwave Theory Techn MTT-38 (January) (1990), pp. 1–7.

[2] M.C. Decreton and F.E. Gardiol, Simple non-destructive method for measurement of complex permittivity, IEEE Trans Instrum Meas IM-23 (December) (1974), pp. 434–438.

[3] N. Qaddoumi, S. Ganchev, G.W. Carriveau and R. Zoughi, Microwave imaging of thick composites with defects, Mater Eval 53 (5) (1995).

[4] P. Venugopalan, K. Jose, K. Nair, P. Chaturvedi and V. Ravindran, Microwave technique for locating inhomogenities in cured rocket propellant samples, NDT Int 19 (6) (1986), pp. 395–397.

[5] A. Bahr, R. Zoughi and N. Qaddoumi, Nondestructive evaluation: theory, techniques, and applications. In: P.J. Shull and M.J. Ehrlich, Editors, Chapter on microwave techniques, an undergraduate introductory text on NDE, Marcel and Dekker, Inc., Publishers (2002), pp. 645–720 April.

[6] R. Zoughi and S. Bakhtiari, Microwave nondestructive detection and evaluation of disbonding and delamination in layered-dielectric slabs, IEEE Trans Instrum Meas 39 (6) (1990), pp. 1059–1063.

[7] Wael Saleh and Nasser Qaddoumi," Potential of Near-Field Microwave Imaging in Breast Cancer Detection Utilizing Tapered Rectangular Waveguide Probes," Proceedings of the 4th IEEE-GCC Conference, Bahrain, Nov. 2007

[8] M. Pastorino, *Microwave imaging*, 1 ed., Hoboken, N.J.: John Wiley, 2010.

[9] R. Justice and V.H. Rumsey, "Measurement of Electric Field Distributions," Institute of Radio Eng. Transactions, AP-3, 1955, pp. 177–180.

[10] J.H. Richmond, "A Modulated Scattering Technique for Measurement of Field Distributions," Microwave Theory and Techniques, IRE Transactions, vol.3, no.4, pp.13-15, July 1955.

[11] D.M. Pozar, *Microwave engineering*, 3 ed., Hoboken, N.J.: John Wiley, 2005.

[12] J.-C. Bolomey, G.E. Gardiol, *Engineering Applications of the Modulated Scatterer Technique*, Norwood, MA: Artech house Inc. 2001.

[13] G. Hygate and J.F. Nye, "Measuring Microwave Fields Directly with an Optically Modulated Scatterer," Measurement Science Technology, Vol. 1, 1990, pp. 703–709.

[14] Kahn W.H., Kurss H., IEEE Trans. Antennas and Propagation, Sept. 1965, p. 671.

[15] Knott E.F., Shaeffer J.F., Tuley M.T., Radar cross Section, Second Edition, Artech house, Boston 1993.

[16] M.T. Ghasr, "Real-time and portable microwave imaging system," Ph.D. dissertation, Dept. Elect. Eng., Missouri univ. of science and technology, 2009.

[17] M.T. Ghasr, M.A. Abou-Khousa, S. Kharkovsky, R. Zoughi and D. Pommerenke, "A Novel 24 GHz One-Shot, Rapid and Portable Microwave Imaging System," Proc. of the IEEE International Instrumentation and Measurement Technology Conference (I2MTC 2008), Victoria, Vancouver Island, Canada, May 12–15, 2008, pp.1798-1802.

[18] S. Caorsi, M. Donelli, M. Pastorino, "A passive antenna system for data acquisition in scattering applications," *IEEE Antennas and Wireless Propagation Letters*, vol.1, no., pp. 203-206, 2002.

[19] A. Franchois, A. Joisel, C. Pichot, J.-C. Bolomey, "Quantitative microwave imaging with a 2.45-GHz planar microwave camera," *IEEE Trans. on Medical Imaging*, vol.17, no.4, pp.550-561, Aug. 1998.

[20] J.-C. Bolomey, G.E. Gardiol, *Engineering applications of the modulated scatterer technique*, Norwood, MA: Artech house Inc. 2001.

[21] M. Converse, E. J. Bond, B. D. Veen, and S. C. Hagness, "A computational study of ultra-wideband versus narrowband microwave hyperthermia for breast cancer treatment", IEEE Transactions on Microwave Theory and Techniques, May 2006.

[22] M. Lazebnik, L. McCartney, D. Popovic, C. B. Watkins, M. J. Lindstrom, J. Harter, S. Sewall, A. Magliocco, J. H. Booske, M. Okoniewski, and S. C. Hagness, "A large-scale study of the ultrawideband microwave dielectric properties of normal breast tissue obtained from reduction surgeries," Physics in Medicine and Biology, Jan. 2007

[23] N. Tavassolian, S. Nikolaou, M. M. Tentzeris, “A Flexible UWB Elliptical Slot Antenna with a Tuning Uneven U-shape Stub on LCP for Microwave Tumor Detection,” Proceedings of Asia-Pacific Microwave Conference, 2007.

[24] Y. J. Kim, L. Joffre, F. De Flaviis, and M. Q. Feng, "3D Microwave imaging technology for damage detection in concrete structures," presented at Proceedings of the International Symposium on Smart Structures and Materials SPIE, Long Beach, 2003.

[25] Wehner, *High resolution radar*. Norwood: Artech House, 1987.

[26] H. Pan, P. Polishuk. *Fiber optics weekly update*. Boston: Information Gatekeepers Inc, p. 298.

[27] R. E. Blahut. *Theory of remote image formation*, United Kingdom: Cambridge University Press, 2004.

[28] T.Y. Yu, O. Buyukozturk. “A far-field radar NDT technique for detecting debonding in gfrp-retrofitted concrete structures,” *NDT&E Intl*, no. 4, pp. 10–24, 2008.

[29] C.A. Balanis, Antenna theory: analysis and design , 3rd ed. Hoboken, New Jersey: Wiley & Sons Inc , 2005.

[30] Transmission Systems for Communications, 3rd ed.,Western Electric Co., Winston-Salem, NC, 1985, pp. 44–60.

[31] Motorola Semiconductor Data Manual, Motorola Semiconductor Products Inc., Phoenix, AZ, 1989

[32] N. Marcuvitz, *Waveguide Handbook*, Peter Peregrinus Ltd, pp. 238-246, UK, 1986.

[33] M. A. Abou-Khousa, S. Kharkovsky, and R. Zoughi, “On the mutual coupling between circular resonant slots”, *Proc. 3nd Intern. Conf. on Electromagnetic (ear-Field Characterization & Imaging (ICO(IC 2007)*, St. Louis, USA, pp. 117 – 122, 2007.

Appendix A

MATLAB CODES

Part a) The code developed for obtaining an image using the range grouping technique

```
clear;clc;
%Open the analog device and channels
if (~isempty(daqfind))
    stop(daqfind);
end
data=0;
jk=1;
Result=zeros(8,8);
test_=zeros(8,8);
while (jk==1);   %infinit loop
    for (i=1:8);% Selecting one column at a time
        AI = analoginput('nidaq','Dev1');%the device and its ID
        chan= addchannel(AI,3);%channel allocation
        SampleRate = 500; % Setting the sample rate
        duration = 0.25; %0.25 second data acquisition time
        set(AI,'SampleRate',SampleRate)
        ActualRate = get(AI,'SampleRate');
        set(AI,'SamplesPerTrigger',duration*ActualRate)
        AI.InputType = 'SingleEnded';
        Fs = ActualRate;
        % Getting the data for each row
        for (j=0:7);
            dio = digitalio('nidaq','Dev1');
            addline(dio,0:5,'out');
            data=j;
            % Control lines
            bvdata = dec2binvec(data,6);
            putvalue(dio,bvdata);
            putvalue(dio.Line(1:6),bvdata);
            start(AI) % Start sampling and storing the input data
            wait(AI,duration+0.1) %Wait for data aquisition to finish
            Data = getdata(AI);
            % The result matrix obtained from averaging all the
samples
            Result(i,j+1)=abs(sum(Data)/(duration*ActualRate));
            Result';
            delete(dio)
            clear dio
            % The calibration vector for a single column
            % test_= [0.0310    0.0293    0.0461    0.0086
0.0562...
            %0.0157    0.0575    0.0011];
```

```
        end
        delete(AI)
        clear AI
    end

    Rez_norm=roundn(Result./test_',-2); %Normalization and rounding
with
                                        %1/100 accuracy

%Range grouping
    for (l=1:8);
        % Due to power source variations, the result signal might go
over
        % the reference signal, thus, if it is higher, the normalized
        % signal has to be set to 1
        if (Rez_norm (l)>1)
            Rez_norm(l)= roundn(test_(l)/Result(l),-2);
        end
        % Signals within other ranges will be normalized as follows
        if (Rez_norm (l) >=0.9)
            Rez_norm(l)=1;
        elseif (Rez_norm(l) >=0.8 && Rez_norm(l) < 0.9 )
            Rez_norm(l)=0.9;
        elseif (Rez_norm(l) >=0.7 && Rez_norm(l) < 0.8 )
            Rez_norm(l)=0.8;
        elseif (Rez_norm(l) >=0.6 && Rez_norm(l) < 0.7 )
            Rez_norm(l)=0.7;
        elseif (Rez_norm(l) >=0.5 && Rez_norm(l) < 0.6 )
            Rez_norm(l)=0.6;
        elseif (Rez_norm(l) >=0.4 && Rez_norm(l) < 0.5 )
            Rez_norm(l)=0.5;
        elseif (Rez_norm(l) >=0.3 && Rez_norm(l) < 0.4 )
            Rez_norm(l)=0.4;
        else
            Rez_norm(l)=0.2;
        end
    end
    subplot(2,1,1:2);
    imagesc(Rez_norm,[0 1]);colormap(jet);colorbar;shg
    xlabel('Row');
    ylabel('Column');

end
```

Part a) The code developed for obtaining an image using the real time generator signal feedback technique. The code for this case is almost the same as that of the previous one with some changes in altering the reference signal.

```
%outputing signal
clear;clc;
%Open the analog device and channels
if (~isempty(daqfind))
    stop(daqfind);
end
data=0;
jk=1;
SampleRate = 500; % Setting the sample rate
FB_duration = 0.1;
duration = 0.25;  % 0.25 second data acquisition time
Result=zeros(8,8);      % Result signal matrix
test_=zeros(8,8);       % Reference matrix
                        % which is to be obtained from the calibratio
Tx_sample= zeros (8,8); % Matrix of the generated signals
                        % which is to be obtained from the
calibration
while (jk==1);  % Infinit loop
    for (i=1:8);% Selecting one column at a time
        % Getting the data for each row
        for (j=0:7);
            % Getting the feedback data from the source
            AI = analoginput('nidaq','Dev1');% The device and its ID
            chan_1= addchannel(AI,2);% Channel allocation
            set(AI,'SampleRate',SampleRate)
            ActualRate = get(AI,'SampleRate');
            set(AI,'SamplesPerTrigger',FB_duration*ActualRate)
            AI.InputType = 'SingleEnded';
            start(AI) % Start sampling and storing the input data
            wait(AI,FB_duration+0.05) %Wait for data aquisition to
finish
            FB_data = getdata(AI);% Feedback data
            delete(AI)
            clear AI
            % Getting the data for the array element
            AI = analoginput('nidaq','Dev1');% The device and its ID
            chan= addchannel(AI,3);% Channel allocation
            set(AI,'SampleRate',SampleRate)
            ActualRate = get(AI,'SampleRate');
            set(AI,'SamplesPerTrigger',duration*ActualRate)
            AI.InputType = 'SingleEnded';
            dio = digitalio('nidaq','Dev1');
            addline(dio,0:5,'out');
            % Control lines
            bvdata = dec2binvec(j+i*8,6);
            putvalue(dio,bvdata);
            putvalue(dio.Line(1:6),bvdata);
            start(AI) % Start sampling and storing the input data
            wait(AI,duration+0.1) %Wait for data aquisition to finish
```

```
            Data = getdata(AI);
            % The signal generated at the source

Tx_feedback(i,j+1)=abs(sum(Data(:,1))/(FB_duration*ActualRate));
            % The result matrix obtained from averaging all the
samples
            Result(i,j+1)=abs(sum(Data(:,2))/(duration*ActualRate));
            delete(dio)
            clear dio
            delete(AI)
            clear AI
            % Checking if the transmitted signal has changed; if so,
the
            % same change will be added to the reference signal
            alter_= Tx_feedback(i,j+1)/Tx_sample(i,j+1);
            if ( alter_ ~= 1)
                if alter > 1;
                    k=-1;
                end
                test_(i,j+1)= test_(i,j+1) - k*alter_*test_(i,j+1);
            end
        end

    end
    difference_=find(Tx_feedback ~= Tx_sample);
    % A sample calibration vector for a single column
    % test_= [0.0310    0.0293    0.0461    0.0086    0.0562...
    %0.0157    0.0575    0.0011];
    Rez_norm=roundn(Result./test_',-2); %Normalization and rounding
with
                                        %1/100 accuracy
    subplot(2,1,1:2);
    imagesc(Rez_norm,[0 1]);colormap(jet);colorbar;shg
    xlabel('Row');
    ylabel('Column');

end
```

VITA

Mohammad Asefi was born on April 10, 1987, in Tehran, Islamic Republic of Iran. He was educated in government and private schools and graduated from Adab Iranian School in 2005. He then got enrolled in the American University of Sharjah, U.A.E, from which he graduated cum laude in 2009. His degree was Bachelor of Science in Electrical Engineering. His design project was on RF energy harvesting for which he submitted three conference proceedings and one peer reviewed journal paper. Mr. Asefi received a graduate teaching assistantship to join the master's program in Electrical Engineering at the American University of Sharjah. His thesis was on Planner Microwave Imaging system and he obtained his M.Sc. degree in June 2011.